Optimal Operation of Water and Power Distribution Networks

Manish K. Singh

Thesis submitted to the Faculty of the
Virginia Polytechnic Institute and State University
in partial fulfillment of the requirements for the degree of

Master of Science
in
Electrical Engineering

Vassilis Kekatos, Chair
Lamine Mili
Walid Saad

December 3, 2018
Blacksburg, Virginia

Keywords: Optimal water flow, distribution system restoration, convex relaxation,
mixed-integer programming, optimal islanding

Optimal Operation of Water and Power Distribution Networks

Manish K. Singh

(ABSTRACT)

Under the envisioned smart city paradigm, there is an increasing demand for the coordinated operation of our infrastructure networks. In this context, this thesis puts forth a comprehensive toolbox for the optimization of electric power and water distribution networks. On the analytical front, the toolbox consists of novel mixed-integer (non)-linear program (MINLP) formulations; convex relaxations with optimality guarantees; and the powerful technique of McCormick linearization. On the application side, the developed tools support the operation of each of the infrastructure networks independently, but also towards their joint operation. Starting with water distribution networks, the main difficulty in solving any (optimal-) water flow problem stems from a piecewise quadratic pressure drop law. To efficiently handle these constraints, we have first formulated a novel MINLP, and then proposed a relaxation of the pressure drop constraints to yield a mixed-integer second-order cone program. Further, a novel penalty term is appended to the cost that guarantees optimality and exactness under pre-defined network conditions. This contribution can be used to solve the WF problem; the OWF task of minimizing the pumping cost satisfying operational constraints; and the task of scheduling the operation of tanks to maximize the water service time in an area experiencing electric power outage. Regarding electric power systems, a novel MILP formulation for distribution restoration using binary indicator vectors on graph properties alongside exact McCormick linearization is proposed. This can be used to minimize the restoration time of an electric system under critical operational constraints, and to enable a coordinated response with the water utilities during outages.

Optimal Operation of Water and Power Distribution Networks

Manish K. Singh

(GENERAL AUDIENCE ABSTRACT)

The advent of smart cities has promoted research towards interdependent operation of utilities such as water and power systems. While power system analysis is significantly developed due to decades of focused research, water networks have been relying on relatively less sophisticated tools. In this context, this thesis develops Advanced efficient computational tools for the analysis and optimization for water distribution networks. Given the consumer demands, an optimal water flow (OWF) problem for minimizing the pump operation cost is formulated. Developing a rigorous analytical framework, the proposed formulation provides significant computational improvements without compromising on the accuracy. Explicit network conditions are provided that guarantee the optimality and feasibility of the obtained OWF solution. The developed formulation is next used to solve two practical problems: the water flow problem, that solves the complex physical equations yielding nodal pressures and pipeline flows given the demands/injections; and an OWF problem that finds the best operational strategy for water utilities during power outages. The latter helps the water utility to maximize their service time during power outages, and helps power utilities better plan their restoration strategy. While the increased instrumentation and automation has enabled power utilities to better manage restoration during outages, finding an optimal strategy remains a difficult problem. The operational and coordination requirements for the upcoming distributed resources and microgrids further complicate the problem. This thesis develops a computationally fast and reasonably accurate power distribution restoration scheme enabling optimal coordination of different generators with optimal islanding. Numerical tests are conducted on benchmark water and power networks to corroborate the claims of the developed formulations.

Dedication

To Guru, Ghar, Desh, and Dost !

Acknowledgments

Let go producing, I could not have understood this work, had I not met my mentor, Dr. Vassilis Kekatos. I sincerely extend my gratitude to him for his continuous efforts in guiding me academically, ethically, and personally. It is the long hours of rigorous meetings that helped me transform my abstract ideas into formal and sound mathematical claims. He has motivated me to take up larger challenges in the field of power systems, and beyond.

I next wish to thank my MS committee members, Dr. Lamine Mili and Dr. Walid Saad for guiding me through the work and motivating me with several possible research directions to proceed with. Apart from this thesis, the confidence that I have gained in power systems comes from the valuable courses and extended discussions with Dr. Chen-Ching Liu, Dr. Lamine Mili and Dr. Virgilio Centeno. I am extremely thankful to them for their support and contributions.

While grad-school is tough, it is surmountable merely because of the *grad-friends*. I thank you all for being a supportive part of good and less good times of my journey so far. I'll be there for you ! Finally, I cannot be more thankful for my family that taught me "*all for one, and one for all*". All that I could do is for you, and because of you. Thank you god, for giving me the people I've got. You are *the* best !

Contents

List of Figures

List of Tables

Chapter 1

Introduction

The ongoing thrust towards smart cities and internet of things has led to a wide-scale deployment of sensors and remote control devices across systems such as power, water, transport, waste-management, security, etc. [1], [2], [3]. The increased situational awareness and controllability as a result, call for enhancing coordinated operation of different infrastructure networks. A few resulting research areas include the gas-electric nexus [4], [5], [6] ; the water-electric nexus [7], [8], [9]; and exploring the cyber-physical inter-dependencies [10]. This thesis is an effort towards the development of a generalized analytical framework for water and power distribution systems, that can give way to solving various optimal coordination problems.

The first main focus of the work presented in this thesis is a novel analytical framework for the analysis of water distribution systems (WDS) [12]. The major challenge in the analysis of WDSs stems from the non-linear equations relating pressure drops to water flows along pipes and the combinatorial formulations for handling discrete on/off decisions. To deal with these challenges, existing approaches resort to linearizations; local non-linear solvers; and/or meta-heuristics; see [12], and the references therein. Alternative approaches result in mixed-integer non-linear problems, which are oftentimes inefficient and feature no global optimality guarantees [11]. However, recent advancements in solving mixed-integer conic-programming motivates development of efficient formulations for (optimal)-water flow yielding feasible solutions with guarantees [13], [34]. Thus, a novel relaxation of the water-flow equations

has been proposed in this thesis, along with a penalty term that yields exact solutions with optimality guarantees under predefined network conditions. The developed framework enables efficiently solving several useful real-world problems. Among these, minimization of pumping cost, maximizing service-time during power outages, and solving the water flow problem have been addressed in this thesis.

The optimal water flow problem that maximizes the service time during power outages helps the power system operators to efficiently design their restoration strategy during outages. This leads us to the second main focus of this thesis which is development of efficient restoration schemes for power distribution systems during outages. While the restoration problem in power distribution systems is quite old, the state-of-the-art has not yet been able to optimally incorporate different types of distributed generators and microgrids, hence limiting the restoration efficacy; see [14] and the references therein. Thus, a power distribution system restoration scheme that optimally incorporates different types of distributed generation has been formulated in this thesis as a mixed-integer linear program.

In general, power distribution system operators perform the system restoration task through sequentially performing switching operations and generation scheduling over a period of time [18]. In such a scenario, oftentimes priorities are placed on restoring different loads based on criticality. Thus, the information of the maximum time a water utility can operate without power supply assists the power utilities to assign suitable priorities to different loads during the restoration process. Thus, the developed analytical frameworks for WDS and power systems lay the path for coordinated operation of the two infrastructure during extreme events.

1.1 Contributions

The primary contribution of this work is a suite of computationally efficient analytical tools that can be used for solving a varied class of optimization problems on water and power distribution systems. The physics governing both water and power networks is based on non-linear non-convex equations. To make these problems tractable, alternate reformulations based on tight convex relaxations are proposed in this thesis. Specifically, the key contributions of this thesis include:

1. A generalized model for various water distribution system components is developed in Section 2.2. The novel model offers distinct features such as separability of binary and continuous variables, flexibility of bypassing pumps, bidirectional flows, and precise tank operation modeling.

2. An OWF problem to minimize electricity operation cost for fixed-speed pumps is formulated in Section 2.3, followed by a convex relaxation yielding an MI-SOCP in Section 2.4.

3. To yield a tight relaxation for the OWF developed in Section 2.4, it is later augmented by a novel penalty term in Section 2.5. Under specific conditions, the penalized relaxation is shown to yield a minimizer of the original non-convex OWF problem.

4. Building upon the model and analytical results of Sections 2.2–2.5, an OWF problem is formulated in Section 2.7 to maximize the service time for a WDS during partial or complete power outages. The exactness of the proposed MI-SOCP relaxation has been validated through numerical tests on a benchmark WDS for numerous problem instances.

5. A single time instant water flow problem is formulated in Section 2.8, and an MI-SOCP

relaxation is proposed. The proposed relaxation is shown to be exact for a moderately sized WDS that grossly violates the restrictive conditions analytically identified to guarantee exactness.

6. A novel power distribution system restoration (DSR) scheme is developed in Chapter 3 as an MILP [14]. The novelty of our DSR stems from the unique use of cycles and paths on the grid infrastructure graph; the McCormick linearization technique; and an approximate power flow model.

7. The DSR scheme finds the optimal formation of islands in a single stage, different from prior works that first identify reference generators and then build islands around them. It further allows for multiple (non)-black-start DGs running on the same island and decides their optimal coordination; and it devises an exact, yet linear model for voltage regulators.

Chapter 2

Optimal Operation of Water Distribution Systems

2.1 Introduction

While WDS serve as a critical infrastructure, there is an increasing emphasis on improving their reliability, quality, and efficiency. The cost-intensive installation and maintenance of WDS components, such as pipelines, pump stations, and reservoirs, have motivated network planning studies [19], [20], [21], [22]. From an operational perspective, a recent survey on WDS optimization identifies pump scheduling and water quality as the two focus areas [11]. Recognizing that 4% of the total electricity consumption in the United States is attributed to water network operations [23], and that the electricity cost for pumping constitutes the largest expenditure for water utilities [24], stresses the significance of optimal WDS scheduling.

A typical WDS schedule would run pumps mainly at night when electricity prices are low to transfer water from reservoirs through pipes and fill up elevated tanks located closer to water demands. Under the smart city vision, dynamic electricity pricing and demand-response programs incentivize more flexible WDS schedules to minimize operational costs. For example, a surplus of residential solar generation around midday could be locally consumed to run pumps and fill up pumps, thus serving as an energy storage alternative. Adaptive

WDS scheduling and the anticipated joint dispatching of electric power and water networks, motivate the need for scalable optimization tools and more realistic system models.

The operation of WDS is constrained by minimum pressure requirements; capacity limitations imposed by pumps, pipelines, and tanks; and a set of hydraulic constraints. It is exactly these hydraulic constraints that give rise to complex mixed-integer and nonlinear formulations, and have been dealt so far in three broad ways [11]. The first class of methods enforces pressure and capacity constraints explicitly, while the hydraulic constraints are included implicitly through water network simulation tools, such as EPANET [25], [26]. Metaheuristic approaches such as genetic algorithms [24], ant-colony optimization [27], or limited discrepancy search [28], are then used together along with a WDS simulator to obtain an operating point. Some variants replace the slow but exact simulator with surrogate WDS models based on artificial neural networks or interpretive structural models [29], [30]. It has been demonstrated however that WDS optimization using metaheuristics coupled with a simulator scales unfavorably due to the computational effort required [31].

The second class of methods rely on formulating (mixed-integer) nonlinear programs and handling them via nonlinear solvers [32]. A mixed-integer second-order cone formulation for optimal pump scheduling relaxes the hydraulic constraints to render the problem convex in the continuous variables [33], [34]. The relaxation is shown to be exact presuming all pipes are equipped with pressure-relieving valves and upon ignoring some pressure tank constraints. The water-power nexus has been studied in [8], wherein the non-convex hydraulic constraints are passed on to a non-convex solver with no optimality guarantees. The security of interdependent water-power-gas networks has been studied from a game-theoretic viewpoint in [35], using the non-convex hydraulic constraints.

The third class of methods uses linearization to end up with a computationally tractable mixed-integer linear program (MILP) formulation [22], [36]. Adopting [34] to find an op-

timal water-power flow dispatch, reference [37] handles the non-convex constraints arising from both water and electric power networks via a successive convex approximation technique. The latter approach features computational advantages without the inaccuracies of linearization; yet water flow directions and the on/off status of pumps are assumed given. The participation of WDS in demand response and frequency regulation through pump scheduling with piece-wise linearization of hydraulic constraints has been suggested in [9], [38], [39].

Towards computationally convenient WDS solvers, the contribution of this chapter is threefold. First, a generalized model for various WDS components is developed in Section 2.2. Some of its distinct features include separability of binary and continuous variables, flexibility of bypassing pumps, bidirectional flows, and precise tank operations modeling. Second, an OWF problem to minimize electricity operation cost for fixed-speed pumps is put forth in Section 2.3. Sections 2.4–2.5 develop a convex relaxation, which is later augmented by a novel penalty term to promote minimizers that are feasible for the water network. Under specific conditions, the penalized relaxation is shown to yield a minimizer of the original non-convex OWF problem. Third, the developed formulation is extended to solve tow practical problems in Sections 2.7–2.8, viz. the water flow problem, and an OWF problem that maximizes the service time of a WDS during a partial/complete power outage in the area. The numerical tests on benchmark WDS corroborate that the proposed relaxations can yield feasible and optimal WDS dispatches even when the analytical conditions are grossly violated.

2.2 Water Network Modeling

A water distribution system can be represented by a directed graph $\mathcal{G}_w := (\mathcal{M}, \mathcal{P})$. Its nodes indexed by $m \in \mathcal{M} := \{1, \ldots, M\}$ correspond to water reservoirs, tanks, and points

of water demand; and its edges in $\mathcal{P}$ with $|\mathcal{P}| = P|$, correspond to water pipes. Reservoirs serve as primary water sources and constitute the subset $\mathcal{M}_r \subset \mathcal{M}$. Similarly, the nodes hosting tanks comprise the subset $\mathcal{M}_b \subset \mathcal{M}$. The nodes in $\mathcal{M}_r \cup \mathcal{M}_b$ do not serve water consumers. This is without loss of generality, since a potential co-located consumer at a node $m \in \mathcal{M}_r \cup \mathcal{M}_b$ can be attached to an auxiliary node connected to the node m through a lossless pipe.

Let d_m^t be the rate of water injected into the network from node m during period t. Apparently, for reservoirs $d_m^t \geq 0$; for demand nodes with water consumers $d_m^t \leq 0$; tanks may be filling or emptying; and for junction nodes $d_m^t = 0$. The directed edge $(m, n) \in \mathcal{P}$ models the pipeline linking nodes m and n. Its water flow will be denoted by d_{mn}^t. If water runs from the node m to n at time t, then $d_{mn}^t \geq 0$; and negative, otherwise. Water flow conservation dictates that

$$d_m^t = \sum_{k:(m,k)\in\mathcal{P}} d_{mk}^t - \sum_{k:(k,m)\in\mathcal{P}} d_{km}^t, \quad \forall m, t. \tag{2.1}$$

In addition to water injections and flows, water distribution system (WDS) operation is also governed by pressures. Water pressure is typically surrogated by the quantity of pressure head, which is measured in meters and is linearly related to water pressure [36]. In detail, a pressure head of h meters corresponds to a water pressure of $h\rho\tilde{g}$ pascal, where ρ is the water density in kg/m^3, assumed to be a known constant and $\tilde{g}$ is the acceleration due to gravity in m/sec^2. The pressure head (also known as piezometric pressure head) at a node equals its geographical elevation plus the manometric pressure head attributed to the height of the water column or pumps.

The pressure head or henceforth simply *pressure* at node m during time t will be denoted by h_m^t. The operation of water networks requires a minimum manometric pressure at all nodes m. Adding this common minimum value of manometric pressure to the specific but known

geographical elevation of each node $m \in \mathcal{M}$ gives a lower limit on its pressure as

$$h_m^t \geq \underline{h}_m. \tag{2.2}$$

Water movement in a pipe results in a quadratic pressure drop. In detail, the pressure drop across pipeline $(m, n) \in \mathcal{P}$ is described by the Darcy-Weisbach equation [36]

$$h_m^t - h_n^t = c_{mn} \operatorname{sign}(d_{mn}^t)(d_{mn}^t)^2 \tag{2.3}$$

where the loss coefficient $c_{mn} := \frac{\ell_{mn} f_{mn}}{4\pi^2 r_{mn}^5 \tilde{g}}$ depends on the pipe length ℓ_{mn}; its inner radius r_{mn}; and the Darcy friction factor f_{mn}. The sign function is defined such as $\operatorname{sign}(0) = 0$ and it ensures that pressure drops in the direction of water flow. To avoid the discontinuity of the sign, we propose a mixed-integer model using the big-M trick for the pressure drop in pipeline (m, n) using the binary variables $\{x_{mn}^t\}_{t=1}^T$. In particular, the pressure drop equation of (2.3) can be equivalently expressed through the constraints

$$-M(1 - x_{mn}^t) \leq d_{mn}^t \leq M x_{mn}^t \tag{2.4a}$$

$$-M(1 - x_{mn}^t) \leq h_m^t - h_n^t - c_{mn}(d_{mn}^t)^2 \leq M(1 - x_{mn}^t) \tag{2.4b}$$

$$-M x_{mn}^t \leq h_m^t - h_n^t + c_{mn}(d_{mn}^t)^2 \leq M x_{mn}^t \tag{2.4c}$$

$$x_{mn}^t \in \{0, 1\} \tag{2.4d}$$

for a large $M > 0$. If $x_{mn}^t = 1$, then constraint (2.4a) guarantees that $d_{mn}^t \geq 0$; constraint (2.4b) becomes an equality; and (2.4c) holds trivially. If $x_{mn}^t = 0$, the flow changes direction $d_{mn}^t \leq 0$; constraint (2.4c) becomes an equality; and (2.4b) holds trivially.

To maintain nodal pressures at desirable levels, water utilities use pumps installed on designated pipes to raise pressure. Let the subset of edges equipped with pumps be denoted

by $\mathcal{P}_a \subset \mathcal{P}$. A water pipe equipped with a pump may be modeled as an ideal lossless pump followed by a pipe with pressure drop dictated by (2.4). Then without loss of generality, all edges $(m,n) \in \mathcal{P}_a$ can be assumed lossless, and the constraints in (2.4) are applied to the set of lossy pipes $\bar{\mathcal{P}}_a := \mathcal{P} \setminus \mathcal{P}_a$.

If pump $(m,n) \in \mathcal{P}_a$ is running during period t, its flow is constrained to lie within the range $\underline{d}_{mn} \leq d^t_{mn} \leq \overline{d}_{mn}$ with $\underline{d}_{mn} \geq 0$ due to engineering limitations [36]. The pump (m,n) adds pressure $g^t_{mn} \geq 0$ so that

$$h^t_n - h^t_m = g^t_{mn}. \tag{2.5}$$

The pressure gain g^t_{mn} depends on the pump speed and the water flow. This dependence is oftentimes approximated by a quadratic function [40], [36], [34]. The dependence of g^t_{mn} on water flow is relatively weak and may be ignored without significant loss of accuracy [34], [41]. Thus, for a fixed-speed pump, the pressure gain g_{mn} is constant when the pump is running; and zero, otherwise. Oftentimes, when a pump is not running, water can flow freely in either directions through a bypass valve connected in parallel to the pump and without incurring any pressure difference [41]. The operation of a pump along with its bypass valve can be captured using the big-M trick via the mixed-integer model for all $(m,n) \in \mathcal{P}_a$

$$h^t_m - h^t_n = -g_{mn} x^t_{mn} \tag{2.6a}$$

$$-M(1 - x^t_{mn}) \leq d^t_{mn} - \tilde{d}^t_{mn} \leq M(1 - x^t_{mn}) \tag{2.6b}$$

$$\underline{d}_{mn} x^t_{mn} \leq \tilde{d}^t_{mn} \leq \overline{d}_{mn} x^t_{mn} \tag{2.6c}$$

$$x^t_{mn} \in \{0,1\}. \tag{2.6d}$$

The binary variable x^t_{mn} indicates whether pump $(m,n) \in \mathcal{P}_a$ is running at time t. When the pump is running ($x^t_{mn} = 1$), constraint (2.6a) implies (2.5); otherwise ($x^t_{mn} = 0$), it enforces $h^t_m = h^t_n$. For $x^t_{mn} = 1$, constraints (2.6b)–(2.6c) imply that $\tilde{d}^t_{mn} = d^t_{mn}$ and the water flow

in the pump is kept within the limits $[\underline{d}_{mn}, \overline{d}_{mn}]$. For $x^t_{mn} = 0$, variable $\tilde{d}^t_{mn}$ is set to zero and d^t_{mn} represents the water flowing through the bypass valve of the pump. The auxiliary variable $\tilde{d}^t_{mn}$ will be useful later in computing the energy consumption of pump (m, n).

Note that a variable-speed pump model is not a generalization of a fixed-speed one unless non-trivial upper and lower bounds on the pump speeds are enforced. For instance, the OWF formulation for variable speed pumps in [34, 37] can not be used for fixed-speed pumps. Although there is an ongoing transition towards variable-speed pumps, the conventional WDS have a fleet of fixed-speed pumps which give way to on/off and implicit flow control [26], [36], [31]. Thus, this work considers fixed-speed pumps.

The pressure at a reservoir can assumed constant across days or weeks [34]. Consider reservoir $m \in \mathcal{M}_r$ whose constant pressure is $\bar{h}_m$. To draw water from this reservoir, its nodal pressure h^t_m must be smaller than the constant pressure head $\bar{h}_m$ of the reservoir. This is enforced through the constraints

$$0 \leq d^t_m \leq M\alpha^t_m \tag{2.7a}$$

$$h^t_m \leq \bar{h}_m + M(1 - \alpha^t_m) \tag{2.7b}$$

$$\alpha^t_m \in \{0, 1\} \tag{2.7c}$$

for all $m \in \mathcal{M}_r$ and times. The binary variable α^t_m indicates if water is drawn from reservoir m at time t. If $\alpha^t_m = 1$, reservoir m is connected to the WDS and the constraints in (2.7) ensure that $d^t_m \geq 0$ and $h^t_m \leq \bar{h}_m$. On the other hand, when $\alpha^t_m = 0$, reservoir m is disconnected, $d^t_m = 0$, and constraint (2.7b) is trivially satisfied.

As opposed to reservoirs, the water volume in tanks varies significantly during the day [34]. Variations in water volume translate to variations in water level, which cause in turn variations in pressure at the bottom of the tank. To model the operation of tanks, let ℓ^t_m

denote the water level in tank $m \in \mathcal{M}_b$ at the end of period t. To be consistent with the piezometric pressure head, the water level ℓ_m^t includes the geographical elevation of tank m. If δ is the duration of a control period and A_m is the uniform cross-sectional area for tank m, the water level in tank m satisfies the dynamics

$$\ell_m^t = \ell_m^{t-1} - \frac{d_m^t \delta}{A_m}. \tag{2.8}$$

Due to its finite volume, the water level in tank m is constrained at all times t as

$$\underline{\ell}_m \leq \ell_m^t \leq \bar{\ell}_m. \tag{2.9}$$

Typically, the net water exchange from tanks is kept at zero during the entire period of operation, that is

$$\ell_m^0 = \ell_m^T. \tag{2.10}$$

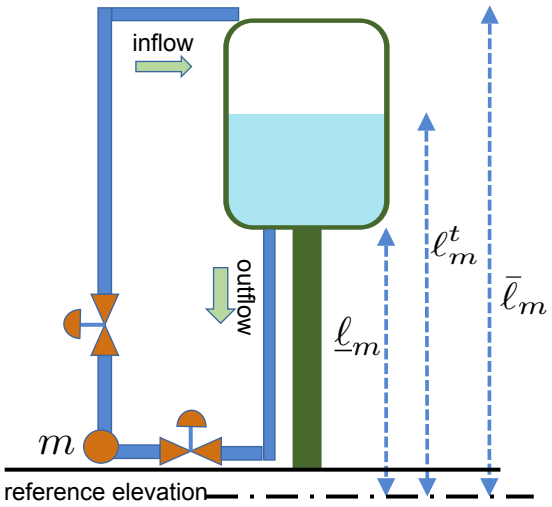

Figure 2.1: A schematic for a water tank sited at node m. The geographical elevation has been incorporated by referring heights to a common reference.

Each tank has two separate paths for filling and emptying; see Fig. 2.1. The filling or inlet pipe is connected near the top, and the emptying or outlet pipe is connected at the bottom.

The two pipes are controlled by two separate valves. The output pressure of the valves can equal or less than the input pressure. Therefore, when tank m is being filled in with water at time t, it should hold $h_m^t \geq \overline{\ell}_m$. Conversely, when water flows out of the tank, it follows that $h_m^t \leq \ell_m^t$. By closing both the inlet and outlet valves, the pressure h_m^t at node m becomes decoupled from the pressure at the bottom of the tank, ℓ_m^t.

To capture the aforementioned tank operation, let us introduce two binary variables (α_m^t, β_m^t) and the auxiliary continuous variable $\tilde{h}_m^t$. The operation of tank m at time t is described by the constraints

$$-M(1-\alpha_m^t) \leq \tilde{h}_m^t - h_m^t \leq M(1-\alpha_m^t) \tag{2.11a}$$

$$-M\alpha_m^t \leq d_m^t \leq M\alpha_m^t \tag{2.11b}$$

$$-M\beta_m^t \leq d_m^t \leq M(1-\beta_m^t) \tag{2.11c}$$

$$\overline{\ell}_m - M(1-\beta_m^t) \leq \tilde{h}_m^t \leq \ell_m^t + M\beta_m^t \tag{2.11d}$$

$$\alpha_m^t, \beta_m^t \in \{0,1\}. \tag{2.11e}$$

The variable α_m^t indicates if tank m is connected at time t; and if it is, the variable β_m^t indicates if the tank is filling. When the tank is connected ($\alpha_m^t = 1$), constraint (2.11a) yields $\tilde{h}_m^t = h_m^t$ and (2.11b) holds trivially. If additionally the tank is filling ($\beta_m^t = 1$), then $d_m^t \leq 0$ from (2.11c) and $\tilde{h}_m^t = h_m^t \geq \overline{\ell}_m$ from (2.11d). If the tank is connected but emptying ($\alpha_m^t = 1, \beta_m^t = 0$), then $d_m^t \geq 0$ from (2.11c) and $\tilde{h}_m^t = h_m^t \leq \ell_m^t$ from (2.11d). When the tank is disconnected ($\alpha_m^t = 0$), constraint (2.11b) enforces $d_m^t = 0$, the pressure in the tank is not related to the network pressure and the value of β_m^t is irrelevant.

Valves are a vital flow-control component. Popular models for valves include an on/off switch model; a linear pressure-reducing model; and a flow-dependent nonlinear model [34]. Presuming a combination of on/off and linear valves on lossy pipes, a convex relaxation for

OWF was put forth in [34]. Although this simplistic setup can be incorporated here, this work addresses the more realistic WDS setup where valves are present only at reservoirs and tanks.

2.3 Optimal Water Flow: Minimizing Pumping Cost

With dynamic pricing, the objective here is to minimize the cost of electricity consumed by water pumps. This section collects the network constraints listed earlier and defines the OWF problem. The mechanical power consumed by pump $(m,n) \in \mathcal{P}_a$ during period t in watts is given by the product of the induced pressure difference g_{mn} measured in pascal, times the water flow $\tilde{d}^t_{mn}$ in m^3/sec [34]. If the overall energy efficiency of the pump is η_{mn}, it consumes electric energy $\frac{\delta\rho\tilde{g}g_{mn}}{\eta_{mn}}\tilde{d}^t_{mn}$ during time t of duration δ. For the fixed-speed pumps considered here, the pressure gain g_{mn} is constant and we can thus define the electricity consumption coefficient

$$c_{mn} := \frac{\delta\rho\tilde{g}g_{mn}}{\eta_{mn}}, \quad \forall (m,n) \in \mathcal{P}_a.$$

The OWF problem can be formally stated as follows. Given the initial water level in tanks $\{\ell^0_m\}_{m\in\mathcal{M}_b}$, the water demands at consumption nodes $\{d^t_m\}_{m\in\mathcal{M}\setminus\mathcal{M}_b\cup\mathcal{M}_r}$, the electricity prices $\{\pi_t\}_{t=1}^T$, and network parameters (tank capacities, pipe dimensions, pump pressure gains and minimum pressure requirements, tank heights); the OWF task aims at minimizing the electricity cost for running the pumps while meeting water demands and respecting WDS limitations.

In detail, the pumping cost can be formulated as

$$f(\tilde{\mathbf{d}}) := \sum_{t=1}^{T} \sum_{(m,n)\in\mathcal{P}_a} c_{mn}\pi_t\tilde{d}^t_{mn} \tag{2.12}$$

where vector $\tilde{\mathbf{d}}$ collects the water flows $\{\tilde{d}_{mn}^t\}_t$ in all pumps $(m,n) \in \mathcal{P}_a$ and at all times. to simplify the presentation, the price of electricity π_t is assumed invariant across the WDS for all t. The OWF problem can be posed as the minimization

$$\begin{aligned} \min \quad & f(\tilde{\mathbf{d}}) && \text{(P1)} \\ \text{over} \quad & \{h_m^t\}_{m\in\mathcal{M}}, \{d_m^t\}_{m\in\mathcal{M}_b\cup\mathcal{M}_r}, \{d_{mn}^t\}_{(m,n)\in\mathcal{P}}, \\ & \{\tilde{h}_m^t\}_{m\in\mathcal{M}_b}, \{\ell_m^t\}_{m\in\mathcal{M}_b}, \{\tilde{d}_{mn}^t\}_{(m,n)\in\mathcal{P}_a}, \\ & \{x_{mn}^t\}_{(m,n)\in\mathcal{P}}, \{\alpha_m^t\}_{m\in\mathcal{M}_r\cup\mathcal{M}_b}, \{\beta_m^t\}_{m\in\mathcal{M}_b}, \quad \forall t \\ \text{s.to} \quad & (2.1), (2.2), (2.4), (2.6) - (2.11). \end{aligned}$$

Problem (P1) involves the continuous variables $\{h_m^t, d_m^t, d_{mn}^t, \tilde{h}_m^t, \tilde{d}_{mn}^t\}$ and the binary variables $\{x_{mn}^t, \alpha_m^t, \beta_m^t\}$. For fixed-speed pumps, the cost in (P1) is linear. Although most of the constraints are linear thanks to the big-M trick, the constraints (2.4b)–(2.4c) modeling the pressure drop are non-linear. In fact, each one of these constraints involves one convex and one non-convex quadratic inequality. To obtain affordable OWF solutions, Section 2.4 relaxes the non-convex constraints and derives a mixed-integer problem that is convex with respect to the continuous variables.

2.4 Convex Relaxation

The pressure drop across a lossy pipe $(m,n) \in \bar{\mathcal{P}}_a$ depends on its water flow d_{mn}^t through the quadratic law of (2.3), which can be relaxed to a convex inequality as

- $h_m^t - h_n^t \geq c_{mn}(d_{mn}^t)^2$ for $d_{mn}^t \geq 0$; or
- $h_n^t - h_m^t \geq c_{mn}(d_{mn}^t)^2$ for $d_{mn}^t \leq 0$.

Since the sign of d_{mn}^t is captured by the binary variable x_{mn}^t, the relaxation can be alternatively performed on (2.4) to yield

$$-M(1-x_{mn}^t) \leq d_{mn}^t \leq M x_{mn}^t \tag{2.13a}$$

$$-M(1-x_{mn}^t) \leq h_m^t - h_n^t - c_{mn}(d_{mn}^t)^2 \tag{2.13b}$$

$$h_m^t - h_n^t + c_{mn}(d_{mn}^t)^2 \leq M x_{mn}^t. \tag{2.13c}$$

Comparing (2.4) to (2.13), the rightmost inequality of (2.4b) and the leftmost inequality of (2.4c) have been dropped in (2.13). There are exactly the non-convex constraints. Replacing (2.4) by (2.13) in (P1), leads to the relaxed problem

$$\begin{aligned} \text{min} \quad & f(\tilde{\mathbf{d}}) \\ \text{over} \quad & \{h_m^t\}_{m\in\mathcal{M}}, \{d_m^t\}_{m\in\mathcal{M}_b\cup\mathcal{M}_r}, \{d_{mn}^t\}_{(m,n)\in\mathcal{P}}, \\ & \{\tilde{h}_m^t\}_{m\in\mathcal{M}_b}, \{\tilde{d}_{mn}^t\}_{(m,n)\in\mathcal{P}_a}, \\ & \{x_{mn}^t\}_{(m,n)\in\mathcal{P}}, \{\alpha_m^t\}_{m\in\mathcal{M}_r\cup\mathcal{M}_b}, \{\beta_m^t\}_{m\in\mathcal{M}_b}, \quad \forall t \\ \text{s.to} \quad & (2.1), (2.2), (2.6)-(2.11), (2.13). \end{aligned} \tag{P2}$$

Problem (P2) is convex with respect to the continuous variables, and it could be handled by existing mixed-integer off-the-shelf solvers. Being a relaxation, the optimal value of (P2) serves as a lower bound for the optimal value of (P1). If a minimizer of (P2) satisfies (2.13b) or (2.13c) with equality for all $(m,n) \in \bar{\mathcal{P}}_a$, the relaxation is deemed *exact*. In this case, the minimizer of (P2) coincides with the minimizer of (P1). Nonetheless, the relaxation is not necessarily exact.

To study the feasible sets of (P1) and (P2), let $\mathbf{h}$ collect the nodal pressures $\{h_m^t\}_{m,t}$; vector $\mathbf{d}$ the water flows $\{d_{mn}^t\}_t$ for all $(m,n) \in \mathcal{P}$; and $\tilde{\mathbf{d}}$ has been defined after (P1). Define the

projection of the feasible set of (P1) into $(\tilde{\mathbf{d}}, \mathbf{d}, \mathbf{h})$ as $\mathcal{S}_1$, and the projection of the feasible set of (P2) into $(\tilde{\mathbf{d}}, \mathbf{d}, \mathbf{h})$ as $\mathcal{S}_2$. The next result shows there exists a bijection between $\mathcal{S}_1$ [resp. $\mathcal{S}_2$] and the feasible set of (P1) [resp. (P2)].

Lemma 2.1. *Any feasible point of* (P1) *and* (P2) *is uniquely characterized by its* $\mathbf{s} := \{\tilde{\mathbf{d}}, \mathbf{d}, \mathbf{h}\}$ *components.*

Proof. It will be shown that upon fixing $(\tilde{\mathbf{d}}, \mathbf{d}, \mathbf{h})$, the remaining variables listed under (P1)–(P3) can be determined. Given $\mathbf{d}$, the water injections $\{d_n^t\}_{n,t}$ are set by (2.1), and subsequently, the water levels $\{\ell_m^t\}_{m,t}$ are set by (2.8). The binary variables capturing flow directions in lossy pipes are

$$x_{mn}^t = \left\lfloor \frac{\operatorname{sign}(d_{mn}^t) + 1}{2} \right\rfloor, \quad \forall (m,n) \in \bar{\mathcal{P}}_a, t$$

where $\lfloor a \rfloor$ denotes the floor function. Likewise, the binary variables characterizing flow directions in pumps are set as $x_{mn}^t = \operatorname{sign}(\tilde{d}_{mn}^t)$ for $(m,n) \in \mathcal{P}_a$.

The variables governing reservoirs and tanks are set as

$$\alpha_m^t = |\operatorname{sign}(d_m^t)|, \quad \forall m \in \mathcal{M}_b \tag{2.14a}$$

$$\beta_m^t = \left\lfloor \frac{1 - \operatorname{sign}(d_m^t)}{2} \right\rfloor, \quad \forall m \in \mathcal{M}_b \tag{2.14b}$$

$$\tilde{h}_m^t = \alpha_m^t h_m^t, \quad \forall m \in \mathcal{M}_b. \tag{2.14c}$$

If tank m is disconnected at time t, then $\alpha_m^t = 0$ and the values of β_m^t and $\tilde{h}_m^t$ become inconsequential. Thus, the unique mapping suggested in (2.14) does not harm feasibility. □

Lemma 2.1 asserts that (P1) and (P2) can be equivalently expressed only in terms of $\mathbf{s} := \{\tilde{\mathbf{d}}, \mathbf{d}, \mathbf{h}\}$. The remaining variables have been introduced merely to avoid discontinuous

or non-differentiable functions (e.g., sign or absolute value) as well as products between continuous and binary variables. In light of Lemma 2.1 and with a slight abuse in terminology, we will henceforth refer to $\mathcal{S}_1$ [resp. $\mathcal{S}_2$] as the *feasible set* of (P1) [resp. (P2)]. Due to the relaxation, it holds $\mathcal{S}_1 \subseteq \mathcal{S}_2$.

When it comes to (P1), a feasible point can be constructed only by its $\{\tilde{\mathbf{d}}, \mathbf{d}\}$ components, since a feasible pressure vector $\mathbf{h}$ can be recovered from $\{\tilde{\mathbf{d}}, \mathbf{d}\}$ as follows. Given $\{\tilde{\mathbf{d}}, \mathbf{d}\}$, the variables $\{x_{mn}^t, \alpha_m^t, \beta_m^t, d_m^t, \ell_m^t\}$ can be set as in the proof of Lemma 2.1. The values of *pressure differences* across pipes can be found by (2.4) and (2.6a). The next question is how to recover pressures from pressure differences.

To express pressure differences at time $t = 1, \ldots, T$, we need to define an edge-node incidence matrix depending on the water flow directions at time t. Define $\mathbf{d}^t$ as the subvector of $\mathbf{d}$ collecting water flows only at time t. Then, introduce the $P \times M$ incidence matrix $\mathbf{A}(\mathbf{d}^t)$ so that if its p-th row corresponds to pipe $p = (m, n)$, then its (p, k) entry is

$$A_{p,k}(\mathbf{d}^t) := \begin{cases} -\operatorname{sign}^2(d_{mn}^t) + \operatorname{sign}(d_{mn}^t) + 1 & , \ k = m \\ \operatorname{sign}^2(d_{mn}^t) - \operatorname{sign}(d_{mn}^t) - 1 & , \ k = n \\ 0 & , \ \text{otherwise.} \end{cases}$$

In this way, vector $\mathbf{A}(\mathbf{d}^t)\mathbf{h}^t$ captures the pressure differences taken across the direction of flow. For zero flows, the standard pipe direction (m, n) is selected without loss of generality.

If $(\mathbf{h}^t, \tilde{\mathbf{d}}^t)$ are the subvectors of $(\mathbf{h}, \tilde{\mathbf{d}})$ corresponding to time t, the pressure differences can be expressed as

$$\mathbf{A}(\mathbf{d}^t)\mathbf{h}^t = \mathbf{b}(\tilde{\mathbf{d}}^t, \mathbf{d}^t), \quad \forall t \tag{2.15}$$

where $\mathbf{b}(\tilde{\mathbf{d}}^t, \mathbf{d}^t)$ is the mapping induced by (2.4) and (2.6a). Since $\{\tilde{\mathbf{d}}, \mathbf{d}\}$ is feasible for (P1), the overdetermined system in (2.15) is consistent. However, its solution is not unique: The

all-one vector $\mathbf{1}$ belongs to the nullspace of $\mathbf{A}(\mathbf{d}^t)$ by definition, so if $\mathbf{h}^t$ satisfies (2.15), then $\mathbf{h}^t + c\mathbf{1}$ satisfies (2.15) too for any c.

Satisfying (2.15) alone is not sufficient for $\mathbf{h}^t$ to be feasible for (P1). It should also satisfy the inequality constraints (2.2), (2.7b), (2.11a), and (2.11d), which are abstractly expressed as

$$\underline{\mathbf{h}}(\tilde{\mathbf{d}}, \mathbf{d}) \leq \mathbf{h} \leq \overline{\mathbf{h}}(\tilde{\mathbf{d}}, \mathbf{d}). \tag{2.16}$$

Given $\{\tilde{\mathbf{d}}, \mathbf{d}\}$ for a feasible point of (P1), a feasible pressure vector $\mathbf{h}$ can be found by ensuring (2.15)–(2.16). A water utility would implement $\mathbf{h}$ by controlling the pressures at reservoir valves. The aforesaid procedure proves the following claim.

Lemma 2.2. *Any feasible point of* (P1) *is characterized by its* $\{\tilde{\mathbf{d}}, \mathbf{d}\}$ *components. A vector of feasible pressures* $\mathbf{h}$ *can be recovered by solving the linear program (LP)*

$$\begin{aligned} &\text{find } \mathbf{h} \\ &\text{s.to } (2.15) - (2.16). \end{aligned} \tag{2.17}$$

Let $\mathcal{H}(\tilde{\mathbf{d}}, \mathbf{d})$ be the set of vectors $\mathbf{h}$ solving the feasibility problem in (2.17). Lemma 2.2 implies that any solution to (2.17) provides a feasible point for (P1).

Given Lemma 2.2, let us see if one can find a feasible point for (P1) by solving (P2). Consider a minimizer $\mathbf{s}_1 = \{\tilde{\mathbf{d}}_1, \mathbf{d}_1, \mathbf{h}_1\}$ of (P1) attaining the cost $f_1 := f(\tilde{\mathbf{d}}_1)$; and a minimizer $\mathbf{s}_2 = \{\tilde{\mathbf{d}}_2, \mathbf{d}_2, \mathbf{h}_2\}$ of (P2) with $f_2 := f(\tilde{\mathbf{d}}_2)$ with $f_2 \leq f_1$ due to the relaxation. The next cases can be identified:

C1. If the relaxation is exact, then $\mathbf{h}_2 \in \mathcal{H}(\tilde{\mathbf{d}}_2, \mathbf{d}_2)$, the costs agree $f_2 = f_1$, and $\mathbf{s}_2$ can be implemented in lieu of $\mathbf{s}_1$.

C2. If the relaxation is inexact, $\mathbf{h}_2$ satisfies only the equations in (2.15) related to pumps, whereas some of the constraints related to lossy pipes in (2.13) are satisfied with strict inequalities. In this case, one may try to recover a vector of WDS-feasible pressures by enforcing (2.15)–(2.16). The following subcases are identified.

C2.a. The linear system of (2.15) is *consistent* for $\mathbf{b}(\tilde{\mathbf{d}}_2, \mathbf{d}_2)$. Again, two cases can be identified.

C2.a.i. The LP in (2.17) is feasible for $(\tilde{\mathbf{d}}_2, \mathbf{d}_2)$ with $\check{\mathbf{h}}_2 \in \mathcal{H}(\tilde{\mathbf{d}}_2, \mathbf{d}_2)$. The point $\check{\mathbf{s}}_2 := \{\tilde{\mathbf{d}}_2, \mathbf{d}_2, \check{\mathbf{h}}_2\}$ is feasible for (P1) and attains the cost $\check{f}_2 := f(\tilde{\mathbf{d}}_2) = f_2$. Because $\check{\mathbf{s}}_2$ is feasible for (P1), the optimal cost has been attained, i.e., $\check{f}_2 = f_2 = f_1$.

C2.a.ii. The LP in (2.17) is infeasible for $(\tilde{\mathbf{d}}_2, \mathbf{d}_2)$. A feasible point for (P1) cannot be recovered.

C2.b. The linear system of (2.15) is *inconsistent* for $\mathbf{b}(\tilde{\mathbf{d}}_2, \mathbf{d}_2)$. A feasible point for (P1) cannot be recovered.

Cases *C1* and *C2.a.i* are computationally useful since they recover an optimal point. Cases *C2.a.ii* and *C2.b* on the other hand, do not provide any practically useful output. Based on numerical tests with different WDS networks and under various pricing/demand scenarios, we have empirically observed that:

- Case *C1* occurs rarely.
- Case *C2.a.i* is encountered frequently in radial networks.
- Case *C2.a.ii* occurs frequently in meshed networks.

Spurred by these observations and to improve the chances for an exact relaxation of (P1),

the next section adds a penalization term in the objective of (P2) and studies the feasibility and optimality of this penalized convex relaxation.

2.5 Penalized Convex Relaxation

Toward an exact relaxation of (P1), define the penalty

$$g(\mathbf{h}) := \sum_{t=1}^{T} \sum_{(m,n)\in\bar{\mathcal{P}}_a} |h_m^t - h_n^t| \tag{2.18}$$

which sums up the absolute pressure differences across lossy pipes and over all times. Let us formulate a *penalized convex relaxation* by replacing the cost of (P2) by

$$\begin{aligned} \min \quad & f(\tilde{\mathbf{d}}) + \lambda g(\mathbf{h}) \\ \text{s.to} \quad & (2.1), (2.2), (2.6) - (2.11), (2.13) \end{aligned} \tag{P3}$$

for $\lambda > 0$. We next study the feasibility and optimality of (P3).

2.5.1 Improving Feasibility

Although (P2) and (P3) share the same feasible set, this section shows that (P3) features two advantages over (P2):

a1) Problem (P3) eliminates the unfavorable case *C2a-i*. The problem instances falling under *C2a-i* with (P2), fall under the useful case *C1* for (P3).

a2) Under some conditions, problem (P3) does not encounter the unfavorable case *C2b* either.

Starting with advantage *a1)*, the following result shown in the appendix is presented first.

Theorem 2.3. *If* $\mathbf{s}_3 := \{\tilde{\mathbf{d}}_3, \mathbf{d}_3, \mathbf{h}_3\}$ *is a minimizer of* (P3) *and* $\mathcal{H}(\tilde{\mathbf{d}}_3, \mathbf{d}_3)$ *is non-empty, then* $\mathbf{h}_3 \in \mathcal{H}(\tilde{\mathbf{d}}_3, \mathbf{d}_3)$.

Proof. Being a minimizer, $\tilde{\mathbf{s}}_3$ is also feasible for (P3). A feasible point of (P3) satisfies only those equations in (2.15) related to pumps. The equality constraints in (2.15) corresponding to lossy pipes are replaced by one-sided linear *inequality* constraints in (P3). To express these facts in a matrix-vector notation, partition $\mathbf{A}(\mathbf{d}^t)$ into submatrix $\mathbf{A}_p(\mathbf{d}^t)$ having the rows of $\mathbf{A}(\mathbf{d}^t)$ related to pumps; and submatrix $\mathbf{A}_l(\mathbf{d}^t)$ having the rows related to lossy pipes. The rows of $\mathbf{A}(\mathbf{d}^t)$ can be permuted without loss of generality so that

$$\mathbf{A}(\mathbf{d}^t) = \begin{bmatrix} \mathbf{A}_p(\mathbf{d}^t) \\ \mathbf{A}_l(\mathbf{d}^t) \end{bmatrix}. \tag{2.19}$$

Likewise, the mapping $\mathbf{b}(\tilde{\mathbf{d}}^t, \mathbf{d}^t)$ in (2.15) can be partitioned into $\mathbf{b}_p(\tilde{\mathbf{d}}^t)$ and $\mathbf{b}_l(\mathbf{d}^t)$. A vector $\mathbf{h}$ is feasible for the relaxed problem (P3) if instead of (2.15), it satisfies

$$\mathbf{A}_p(\mathbf{d}^t)\mathbf{h}^t = \mathbf{b}_p(\tilde{\mathbf{d}}^t), \quad \forall t \tag{2.20a}$$

$$\mathbf{A}_l(\mathbf{d}^t)\mathbf{h}^t \geq \mathbf{b}_l(\mathbf{d}^t) \geq \mathbf{0}, \quad \forall t. \tag{2.20b}$$

Granted $\mathcal{H}(\tilde{\mathbf{d}}_3, \mathbf{d}_3)$ is non-empty by hypothesis, there exists an $\check{\mathbf{h}}_3 \in \mathcal{H}(\tilde{\mathbf{d}}_3, \mathbf{d}_3)$ so that $\check{\mathbf{s}}_3 := \{\tilde{\mathbf{d}}_3, \mathbf{d}_3, \check{\mathbf{h}}_3\}$ satisfies (2.15)–(2.16). Because $\check{\mathbf{s}}_3$ satisfies (2.15), it satisfies the constraints (2.20b) with equality. Thus, vector $\check{\mathbf{s}}_3$ is feasible for (P3). Moreover, the cost of (P3) for $\check{\mathbf{s}}_3$ is $f(\tilde{\mathbf{d}}_3)+\lambda g(\check{\mathbf{h}}_3) = f_3+\lambda\sum_{t=1}^{T}\|\mathbf{A}_l(\mathbf{d}_3^t)\check{\mathbf{h}}_3^t\|_1$, where $f_3 := f(\tilde{\mathbf{d}}_3)$, and $\check{\mathbf{h}}_3^t$ and $\mathbf{d}_3^t$ are accordingly the subvectors of $\check{\mathbf{h}}_3$ and $\mathbf{d}_3$ collecting the entries corresponding to time t. Since $\check{\mathbf{s}}_3$ satisfies (2.20b) with equality, the cost becomes $f_3 + \lambda\sum_{t=1}^{T}\|\mathbf{b}_l(\mathbf{d}_3^t)\|_1$.

Proving by contradiction, suppose $\mathbf{h}_3 \notin \mathcal{H}(\tilde{\mathbf{d}}_3, \mathbf{d}_3)$. This implies $\mathbf{h}_3$ does not satisfy the left-hand side of (2.20b) with equality. Instead, there exists a sequence of $\boldsymbol{\epsilon}^t \geq \mathbf{0}$, such that $\mathbf{A}_l(\mathbf{d}_3^t)\mathbf{h}_3^t = \mathbf{b}_l(\mathbf{d}_3^t) + \boldsymbol{\epsilon}^t$ for all t and $\sum_{t=1}^T \boldsymbol{\epsilon}^t \neq \mathbf{0}$. Evaluating the objective of (P3) for the minimizer $\mathbf{s}_3$ yields

$$\begin{aligned} f(\tilde{\mathbf{d}}_3) + \lambda g(\tilde{\mathbf{h}}_3) &= f_3 + \lambda \sum_{t=1}^T \|\mathbf{A}_l(\mathbf{d}_3^t)\mathbf{h}_3^t\| \\ &= f_3 + \lambda \sum_{t=1}^T \left(\|\mathbf{b}_l^t(\mathbf{d}_3^t)\|_1 + \|\boldsymbol{\epsilon}_t\|_1\right) \\ &> f_3 + \lambda \sum_{t=1}^T \|\mathbf{b}_l^t(\mathbf{d}_3^t)\|_1 \end{aligned}$$

where the second equality stems from $\mathbf{b}_l(\mathbf{d}^t) \geq \mathbf{0}$ and $\boldsymbol{\epsilon}_t \geq \mathbf{0}$ for all t; and the strict inequality holds because $\lambda > 0$ and $\sum_{t=1}^T \boldsymbol{\epsilon}^t \neq \mathbf{0}$. This inequality contradicts the optimality of $\mathbf{s}_3$, and nullifies the hypothesis that $\mathbf{h}_3 \notin \mathcal{H}(\tilde{\mathbf{d}}_3, \mathbf{d}_3)$. □

From Theorem 2.3 and Lemma 2.2, the next result follows.

Corollary 2.4. *Under the assumptions of Theorem 2.3, the minimizer* $\mathbf{s}_3 := \{\tilde{\mathbf{d}}_3, \mathbf{d}_3, \mathbf{h}_3\}$ *of* (P3) *is feasible for* (P1).

Corollary 2.4 asserts that if the water flows obtained via (P3) can be mapped to physically feasible pressures, then the minimizer of (P3) contains already physically feasible pressures and this shows advantage *a1)*.

Before moving to *a2)*, some graph theory preliminaries are reviewed. Given an undirected graph $\mathcal{G} := (\mathcal{M}, \mathcal{P})$, the *degree* is the number of incident edges. A graph is connected if there exists a sequence of adjacent edges between any two of its nodes. A minimal set of edges $\mathcal{P}_\mathcal{T}$ preserving the connectivity of a connected graph constitutes a *spanning tree* of $\mathcal{G}$; is denoted by $\mathcal{T} := (\mathcal{M}, \mathcal{P}_\mathcal{T})$; and apparently, $|\mathcal{P}_\mathcal{T}| = |\mathcal{M}| - 1$. The edges not belonging to a spanning

tree $\mathcal{T}$ are referred to as *links* with respect to $\mathcal{T}$. A *cycle* is a sequence of adjacent edges without repetition that starts and begins at the same node. A *tree* is a connected graph with no cycles. In a directed graph, each edge is assigned a directionality. A *path* from node m to n is defined as a sequence of directed edges originating from m and terminating at n. Given the undirected graph $(\mathcal{M}, \mathcal{P})$ modeling a WDS and the vector $\mathbf{d}^t$ of flows at time t, let us define the *directed* graph $(\mathcal{M}, \mathcal{P}(\mathbf{d}^t))$ where edge p runs from node m to node n if $d^t_{m,n} \geq 0$; and vice versa, otherwise.

To show *a2)*, we study the consistency of (2.15). Had the WDS graph been a tree, the edge-node incidence matrix would have been full row-rank [42], and hence (2.15) consistent for any $\mathbf{b}(\tilde{\mathbf{d}}^t, \mathbf{d}^t)$. This implies that possible inconsistencies in (2.15) arise from cycles in the WDS graph. Because studying the generic case of cycles is not obvious, we consider the special case of a cycle where all but one nodes have degree two. This subset of edges will be henceforth termed a *ring* rooted at the node with degree larger than two. We provide conditions under which a minimizer of (P3) satisfies the constraints in (2.13) with equality for all edges of a ring.

Lemma 2.5. *Let* $\mathbf{s}_3 = \{\tilde{\mathbf{d}}_3, \mathbf{d}_3, \mathbf{h}_3\}$ *be a minimizer of* (P3) *and* $\mathbf{d}^t_3$ *be the subvector of* $\mathbf{d}_3$ *collecting the flows at time* t*. If the directed graph* $(\mathcal{M}, \mathcal{P}(\mathbf{d}^t_3))$ *contains a ring* $\mathcal{R} \subseteq \mathcal{P}(\mathbf{d}^t_3)$ *rooted at node* m*, such that*

- *all nodes incident to* $\mathcal{R}$ *have identical pressure limit* $\underline{h}$*;*
- *all nodes incident to* $\mathcal{R}$ *but* m *host no tanks or reservoirs;*
- *all edges in* $\mathcal{R}$ *host no pumps;*

then $h^t_i - h^t_j = c_{ij}(d^t_{ij})^2$ *for all directed edges* (i, j) *in* $\mathcal{R}$*.*

Proof. Since this proof refers to a particular time, the superscript t is omitted for simplicity. Given a point $\{\tilde{\mathbf{d}}, \mathbf{d}, \mathbf{h}\}$, an edge will be termed (in)exact if constraint (2.13) is satisfied with (in)equality for that point. Since all nodes incident to $\mathcal{R}$ excluding m host no tanks or reservoirs, they must have non-positive injections. Therefore, its two incident edges cannot both have outgoing water flows from (2.1). This implies that the ring can either consist of two parallel paths, or a directed cycle. In the latter case, adding the constraints $h_i - h_j \geq c_{ij}(d_{ij})^2$ around $\mathcal{R}$ would give $\sum_{(i,j)\in\mathcal{R}} c_{ij} d_{ij}^2 \leq h_m - h_m = 0$, implying $d_{ij} = 0$ for all edges in $\mathcal{R}$, which is a contradiction. Thus, the ring $\mathcal{R}$ consists of two parallel paths from m to some node n, henceforth termed $\mathcal{P}_1$ and $\mathcal{P}_2$.

The rest of the proof proceeds in two steps. The first step shows there exists a minimizer of (P3) with at most one inexact edge in $\mathcal{R}$. The second step reduces the number to none.

For the first step, we will modify the pressure vector in $\mathbf{s}_3$ to construct $\hat{\mathbf{s}}_3 := \{\tilde{\mathbf{d}}_3, \mathbf{d}_3, \hat{\mathbf{h}}_3\}$ for which there exists at most one inexact edge in $\mathcal{R}$. The new point $\hat{\mathbf{s}}_3$ is feasible for (P3) and attains smaller or equal cost than $\mathbf{s}_3$. To do so, for each node k incident to $\mathcal{R}$ excluding m and n, assign the pressure consistent with (2.3) along the path $\mathcal{P}_{mk}$ from m to k:

$$\hat{h}_k := h_m - \sum_{(i,j)\in\mathcal{P}_{mk}} c_{ij} d_{ij}^2 \geq h_k \geq \underline{h}$$

where the first inequality stems from summing up the constraints $h_i - h_j \geq c_{ij} d_{ij}^2$ for all edges (i, j) along $\mathcal{P}_{mk}$, and guarantees that $\hat{h}_k$ is feasible.

For the terminal node n, assign the pressure

$$\hat{h}_n := \min_{l\in\{1,2\}} \Big\{ h_m - \sum_{(i,j)\in\mathcal{P}_l} c_{ij} d_{ij}^2 \Big\}. \tag{2.21}$$

Adding the constraints $h_i - h_j \geq c_{ij} d_{ij}^2$ for all edges (i,j) in $\mathcal{P}_l$ and $\mathcal{P}_2$ separately, yields

$$h_m - h_n \geq \sum_{(i,j)\in\mathcal{P}_l} c_{ij} d_{ij}^2, \quad l \in \{1,2\}. \tag{2.22}$$

Hence, we get that

$$h_n \leq \min_{l\in\{1,2\}} \left\{ h_m - \sum_{(i,j)\in\mathcal{P}_l} c_{ij} d_{ij}^2 \right\} = \hat{h}_n \tag{2.23}$$

implying $\hat{h}_n \geq h_n \geq \underline{h}$.

Since the pressures on the nodes within $\mathcal{R}$ have been increased and they are not upper bounded in the absence of tanks or reservoirs, the point $\hat{\mathbf{s}}_3$ is feasible. The difference in the objective of (P3) attained by $\mathbf{s}_3$ and $\hat{\mathbf{s}}_3$ is

$$\begin{aligned} &f(\tilde{\mathbf{d}}_3) + \lambda g(\mathbf{h}_3) - f(\tilde{\mathbf{d}}_3) - \lambda g(\hat{\mathbf{h}}_3) \\ &= \lambda \sum_{(i,j)\in\mathcal{R}} \left(|h_i - h_j| - |\hat{h}_i - \hat{h}_j| \right). \end{aligned}$$

Since all directed edges in $\mathcal{P}_1$ and $\mathcal{P}_2$ have positive flows

$$\begin{aligned} \sum_{(i,j)\in\mathcal{R}} |h_i - h_j| &= \sum_{(i,j)\in\mathcal{P}_1} (h_i - h_j) + \sum_{(i,j)\in\mathcal{P}_2} (h_i - h_j) \\ &= 2(h_m - h_n). \end{aligned}$$

Applying the same argument for $\hat{\mathbf{h}}_3$, it follows that

$$f(\tilde{\mathbf{d}}_3) + \lambda g(\mathbf{h}_3) - f(\tilde{\mathbf{d}}_3) - \lambda g(\hat{\mathbf{h}}_3) = 2\lambda(\hat{h}_n - h_n) \geq 0. \tag{2.24}$$

If for $\mathbf{s}_3$ there exist inexact edges in both $\mathcal{P}_1$ and $\mathcal{P}_2$, then (2.22) holds with strict inequality for both paths. It follows from (2.23) that $\hat{h}_n > h_n$, and so $\hat{\mathbf{s}}_3$ contradicts the optimality of

$\mathbf{s}_3$. This proves that all inexact edges in $\mathcal{R}$ must belong exclusively to $\mathcal{P}_1$ or $\mathcal{P}_2$. In the latter case, the inequality in (2.23) holds with equality, and from (2.24) the point $\hat{\mathbf{s}}_3$ becomes a minimizer of (P3). Note $\hat{\mathbf{s}}_3$ has at most one inexact edge in $\mathcal{R}$, and that is the last edge in $\mathcal{P}_1$ or $\mathcal{P}_2$.

For the second step of this proof and proving by contradiction, suppose there exist exactly one inexact edge for the minimizer $\mathbf{s}_3$ in $\mathcal{P}_1$. That means that (2.22) holds with inequality for $l = 1$, and equality for $l = 2$, implying

$$\sum_{(i,j)\in\mathcal{P}_1} c_{ij} d_{ij}^2 < \sum_{(i,j)\in\mathcal{P}_2} c_{ij} d_{ij}^2. \tag{2.25}$$

From $\mathbf{d}_3$, construct a water flow vector $\check{\mathbf{d}}_3$ with entries

$$\check{d}_{ij} = \begin{cases} d_{ij} + \epsilon & , \ (i,j) \in \mathcal{P}_1 \\ d_{ij} - \epsilon & , \ (i,j) \in \mathcal{P}_2 \\ d_{ij} & , \ (i,j) \in \mathcal{P} \setminus (\mathcal{P}_1 \cup \mathcal{P}_2) \end{cases} \tag{2.26}$$

for some $\epsilon > 0$. This redistribution of flows satisfies (2.1). Moreover, for increasing ϵ, the LHS of (2.25) increases and the RHS decreases. This is because $c_{ij} d_{ij}^2$ is an increasing function for positive d_{ij}. The goal is to select ϵ, so that

$$\sum_{(i,j)\in\mathcal{P}_1} c_{ij} \check{d}_{ij}^2 = \sum_{(i,j)\in\mathcal{P}_2} c_{ij} \check{d}_{ij}^2 < \sum_{(i,j)\in\mathcal{P}_2} c_{ij} d_{ij}^2. \tag{2.27}$$

While increasing ϵ to achieve (2.27), some of the $\{\check{d}_{ij}\}_{(i,j)\in\mathcal{P}_2}$ may become negative. This case is ignored for now.

Construct next a new pressure vector $\check{\mathbf{h}}_3$ by changing the entries of $\mathbf{h}_3$ corresponding to the

non-root nodes in $\mathcal{R}$ as

$$\check{h}_k := h_m - \sum_{(i,j)\in\mathcal{P}_{mk}} c_{ij}\check{d}_{ij}^2. \tag{2.28}$$

For $k = n$, the sum in the RHS of (2.28) can be evaluated over $\mathcal{P}_1$ or $\mathcal{P}_2$, since these two sums are equal from (2.27). The constructed pressures for nodes incident to $\mathcal{R}$ satisfy

$$\check{h}_k \geq \check{h}_n > h_n \geq \underline{h}. \tag{2.29}$$

The first inequality holds because node n has the largest value for the sum in (2.28); and the second inequality because

$$\check{h}_n = h_m - \sum_{(i,j)\in\mathcal{P}_2} c_{ij}\check{d}_{ij}^2 > h_m - \sum_{(i,j)\in\mathcal{P}_2} c_{ij}d_{ij}^2 = h_n.$$

The inequalities in (2.29) prove that $\check{\mathbf{h}}_3$, and hence the point $\check{\mathbf{s}}_3 := \{\tilde{\mathbf{d}}_3, \check{\mathbf{d}}_3, \check{\mathbf{h}}_3\}$ is feasible for (P3). The difference in the objective of (P3) attained by $\mathbf{s}_3$ and $\check{\mathbf{s}}_3$ is

$$f(\tilde{\mathbf{d}}_3) + \lambda g(\mathbf{h}_3) - f(\tilde{\mathbf{d}}_3) - \lambda g(\check{\mathbf{h}}_3) = 2\lambda(\check{h}_n - h_n) > 0$$

which contradicts the optimality of $\mathbf{s}_3$.

Since all water injections at non-root nodes over $\mathcal{R}$ are non-positive, the water flows are non-increasing along $\mathcal{P}_2$. This implies that $d_{ij} \geq d_{n_1,n}$ for all $(i,j) \in \mathcal{P}_2$, where (n_1, n) is the last edge of $\mathcal{P}_2$. Thus, by increasing ϵ, the flow $d_{n_1,n}$ may become negative. In that case, the edge (n_1, n) is removed from $\mathcal{P}_2$ and appended to $\mathcal{P}_1$, forming a new pair of parallel paths with n_1 as the new terminal node. The second step of this proof can be repeated on the new parallel paths. □

Leveraging Lemma 2.5, the ensuing result shows the advantage *a2* of (P3) over (P2) for a large class of practical WDS.

Theorem 2.6. *Let* $\mathbf{s}_3 := \{\tilde{\mathbf{d}}_3, \mathbf{d}_3, \mathbf{h}_3\}$ *be a minimizer of* (P3) *and* $(\tilde{\mathbf{d}}_3^t, \mathbf{d}_3^t)$ *be the subvectors of* $(\tilde{\mathbf{d}}_3, \mathbf{d}_3)$ *corresponding to time* t*. The system of equations in* (2.15) *is consistent for* $\mathbf{s}_3$ *at time* t*, if all undirected cycles in* $(\mathcal{M}, \mathcal{P}(\mathbf{d}_3^t))$ *constitute rings satisfying the conditions of Lemma 2.5.*

Proof. Let $\mathcal{T} := (\mathcal{M}, \mathcal{P}_\mathcal{T})$ be a spanning tree of $(\mathcal{M}, \mathcal{P}(\mathbf{d}_3^t))$. Reorder the equations in (2.15) as

$$\begin{bmatrix} \mathbf{A}_\mathcal{T}(\mathbf{d}_3^t) \\ \mathbf{A}_{\bar{\mathcal{T}}}(\mathbf{d}_3^t) \end{bmatrix} \mathbf{h}^t = \begin{bmatrix} \mathbf{b}_\mathcal{T}(\tilde{\mathbf{d}}_3^t, \mathbf{d}_3^t) \\ \mathbf{b}_{\bar{\mathcal{T}}}(\tilde{\mathbf{d}}_3^t, \mathbf{d}_3^t) \end{bmatrix} \tag{2.30}$$

where $\mathbf{A}_\mathcal{T}(\mathbf{d}_3^t)$ and $\mathbf{b}_\mathcal{T}(\tilde{\mathbf{d}}_3^t, \mathbf{d}_3^t)$ are the rows of $\mathbf{A}(\mathbf{d}_3^t)$ and $\mathbf{b}(\tilde{\mathbf{d}}_3^t, \mathbf{d}_3^t)$ corresponding to the edges in $\mathcal{P}_\mathcal{T}$; and $\mathbf{A}_{\bar{\mathcal{T}}}(\mathbf{d}_3^t)$ and $\mathbf{b}_{\bar{\mathcal{T}}}(\tilde{\mathbf{d}}_3^t, \mathbf{d}_3^t)$ the rows corresponding to the edges in $\mathcal{P} \setminus \mathcal{P}_\mathcal{T}$.

Being an edge-node incidence matrix for a tree, matrix $\mathbf{A}_\mathcal{T}(\mathbf{d}_3^t)$ is full row-rank [42], and hence the system $\mathbf{A}_\mathcal{T}(\mathbf{d}_3^t)\mathbf{h}^t = \mathbf{b}_\mathcal{T}(\tilde{\mathbf{d}}_3^t, \mathbf{d}_3^t)$ is consistent. The rows of $\mathbf{A}_{\bar{\mathcal{T}}}(\mathbf{d}_3^t)$ correspond to the links defined by $\mathcal{T}$. By the hypothesis, every undirected cycle in $(\mathcal{M}, \mathcal{P}(\mathbf{d}_3^t))$ is a ring. Then, all but one of its edges belong to $\mathcal{T}$, and the remaining edge belongs to $\bar{\mathcal{T}}$. In fact, every edge in $\bar{\mathcal{T}}$ must belong to a ring. Since by the conditions of Lemma 2.5, no pumps are allowed on a ring, every equation in the bottom part of (2.30) corresponds to a lossy pipeline (k, l) and will be of the form $h_k^t - h_l^t = c_{kl} d_{kl}^2$.

Since we refer to time t, the superscript t is omitted to unclutter notation. Consider link $(k, l) \in \bar{\mathcal{T}}$ that belongs to the pair of parallel paths $\mathcal{P}_1$ and $\mathcal{P}_2$ with origin node m and destination n. Without loss of generality, let also $(k, l) \in \mathcal{P}_1$. From Lemma 2.5, it holds that

$h_i - h_j = c_{ij} d_{ij}^2$ for all $(i,j) \in \mathcal{P}_1 \cup \mathcal{P}_2$. Summing these constraints along $\mathcal{P}_1$ and $\mathcal{P}_2$ yields

$$\sum_{(i,j)\in\mathcal{P}_1} (h_i - h_j) = \sum_{(i,j)\in\mathcal{P}_1} c_{ij} d_{ij}^2 = h_m - h_n \tag{2.31a}$$

$$\sum_{(i,j)\in\mathcal{P}_2} (h_i - h_j) = \sum_{(i,j)\in\mathcal{P}_2} c_{ij} d_{ij}^2 = h_m - h_n \tag{2.31b}$$

so that (2.31a) equals (2.31b). Separating the contribution of edge (k,l) from $\mathcal{P}_1$ in the leftmost and central parts of (2.31a) provides

$$h_k - h_l = \sum_{(i,j)\in\mathcal{P}_2} (h_i - h_j) - \sum_{(i,j)\in\mathcal{P}_1\setminus(k,l)} (h_i - h_j) \tag{2.32a}$$

$$c_{kl} d_{kl}^2 = \sum_{(i,j)\in\mathcal{P}_2} c_{ij} d_{ij}^2 - \sum_{(i,j)\in\mathcal{P}_1\setminus(k,l)} c_{ij} d_{ij}^2. \tag{2.32b}$$

Note that the pressure drop equations along for all edges $(i,j) \in \mathcal{P}_1 \cup \mathcal{P}_2 \setminus (k,l)$ are rows in the system $\mathbf{A}_{\mathcal{T}}(\mathbf{d}_3^t)\mathbf{h}^t = \mathbf{b}_{\mathcal{T}}(\tilde{\mathbf{d}}_3^t, \mathbf{d}_3^t)$. From (2.32), the pressure drop equation corresponding to edge $(k,l) \in \bar{\mathcal{T}}$ has been expressed as a linear combination of the rows of $\mathbf{A}_{\mathcal{T}}(\mathbf{d}_3)\mathbf{h} = \mathbf{b}_{\mathcal{T}}(\tilde{\mathbf{d}}_3, \mathbf{d}_3)$. The argument holds for all equations in the bottom part of (2.30), thus making the overall system in (2.15) consistent. □

To appreciate the claim of Theorem 2.6, recall that for a point to be feasible for (P1), it is sufficient to satisfy (2.15) and (2.16). Since $\mathbf{A}(\mathbf{d}^t)\mathbf{1} = \mathbf{0}$, the next result can be inferred.

Corollary 2.7. *Under the assumptions of Theorem 2.6, if the left or right inequality in (2.16) are omitted, then a minimizer of (P3) is feasible for (P1).*

Corollary 2.7 asserts that (P3) can be advantageous for coping with OWF tasks with no upper bounds on pressures; see also [33]. An important problem complying to this setup is the *water flow* (WF) task. Different from OWF, the WF problem solves the WDS equations over a single period upon specifying nodal water demands and a reference pressure.

2.5.2 Optimality

The previous section documented the advantages of the penalized convex relaxation of (P3) over (P2) in terms of providing physically feasible WDS dispatches. However, the objective in (P3) differs from the one of (P1): If a minimizer $\mathbf{s}_3 = \{\tilde{\mathbf{d}}_3, \mathbf{d}_3, \mathbf{h}_3\}$ of (P3) is feasible for (P1), it will achieve in general a larger pumping cost than a minimizer of (P1), that is $f(\tilde{\mathbf{d}}_3) \geq f_1$. However, this suboptimality gap diminishes for decreasing λ as explained next; see e.g., [43, Sec. 4.7.5].

Lemma 2.8 ([43]). *Consider the minimization problem*

$$\mathbf{x}_\lambda := \text{argmin}_{\mathbf{x}\in\mathcal{X}}\, f(\mathbf{x}) + \lambda g(\mathbf{x}).$$

If $\lambda_2 > \lambda_1 \geq 0$, *then* $f(\mathbf{x}_{\lambda_2}) \geq f(\mathbf{x}_{\lambda_1})$.

Lemma 2.8 implies that for decreasing λ, a minimizer of (P3) gives lower $f(\tilde{\mathbf{d}}_3(\lambda))$. For $\lambda = 0$, problem (P3) degenerates to (P2), and gives a lower bound on f_1. Overall, we get that

$$f(\tilde{\mathbf{d}}_2) \leq f_1 \leq f(\tilde{\mathbf{d}}_3(\lambda)). \tag{2.33}$$

From Theorems 2.3 and 2.6, the advantage of the penalty term $g(\mathbf{h})$ does not depend on the value of $\lambda > 0$. So λ can be chosen arbitrarily small to tighten the second inequality in (2.33). The caveat behind the bounds of (2.33) are the conditions assumed by Lemma 2.5 and Theorem 2.6. Even though these conditions were grossly violated during the tests of Section 2.6, the inequalities in (2.33) were frequently tightened to equalities. Albeit (P2) oftentimes attained the optimal cost f_1, its minimizer was not feasible for (P1). In fact, there is no direct way of converting the minimizer of (P2) to a feasible point. Instead, problem (P3) found a minimizer for (P1) in most tests.

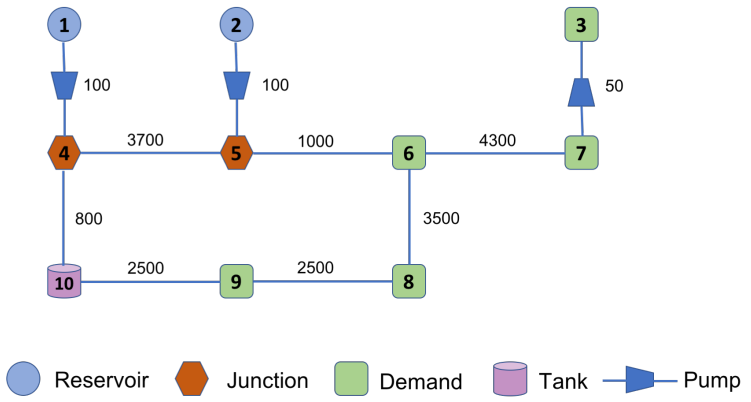

Figure 2.2: Benchmark water distribution system. The length for lossy pipes and head gain for pumps are shown in meters.

2.6 Numerical Tests

The new OWF solver was evaluated on the benchmark WDS of [37], [41], and shown in Figure 2.2. It consists of 10 nodes including 2 reservoirs and a tank; 3 fixed-speed pumps; and 7 lossy pipes. All lossy pipes have a diameter of 0.4 m and friction coefficient $f_{m,n} = 0.01$. The efficiency for all pumps is 85% and for their motors 95%, resulting in an overall efficiency of $\eta = 0.81$. The minimum and maximum water flows for all pumps are 100 m^3/hr and $1,500$ m^3/hr, respectively. The pressure at reservoir nodes 1 and 2 is accordingly -2.5 m and 5 m. The minimum pressure requirement $\underline{h}_m$ for nodes 3 to 10 is $\{10, 7, 12, 10, 5, 10, 10, 10\}$ m. Tank node 10 has an area of $A_{10} = 490.87$ m^2; water level limits $\underline{\ell}_{10} = 10$ and $\overline{\ell}_{10} = 30$ m; and initial water level $\ell_{10}^0 = 20$ m.

The WDS was scheduled hourly for a horizon of $T = 12$ hours for the demands of Figure 2.3; see [37]. The prices $\{\pi_t\}_{t=1}^{12}$ were set to the average day-ahead locational marginal prices during 8:00–20:00 on April 1, 2018 from the PJM market, and are shown in Fig. 2.4. The OWF tests were solved using the MATLAB-based optimization toolbox YALMIP along with the mixed-integer solver Gurobi [44], [45]. All tests were run on a 2.7 GHz, Intel Core i5 computer with 8 GB RAM.

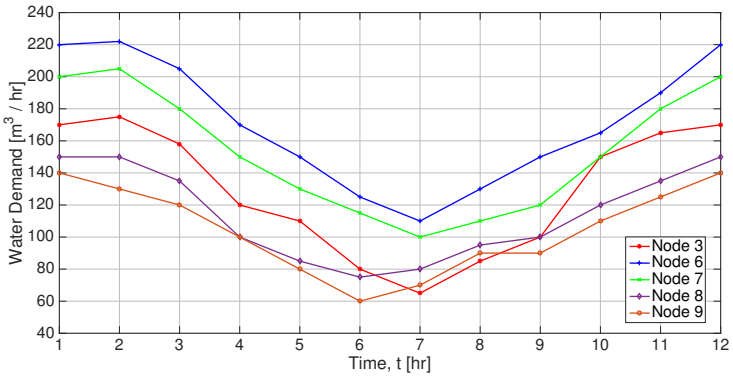

Figure 2.3: Per-node water demand across time.

We first checked whether the convex relaxation was exact. A minimizer of (P3) was deemed feasible for (P1) if $|h_m^t - h_n^t| - c_{mn}\left(d_{mn}^t\right)^2 \leq 10^{-4}$ for all pipes and times. A minimizer for (P3) was obtained in 8.34 sec for $\lambda = 0.1$. The minimizer was in fact feasible for (P1). Figure 2.4 presents the power consumed by pumps (top) and the water level in tank 10 (bottom). The pumps run for the hours with the lowest prices over which tank node 10 is filled, as expected. The tank is emptied during the hours of higher electricity prices, and its level is brought to its initial level at the end of the horizon.

Table 2.1: Pumping cost attained by a minimizer of (P3) for different λ

λ	0	0.01	0.1	1
$f(\tilde{\mathbf{d}}_3)$	5,699.0	5,699.0	5,699.0	5,704.2
comment	lower bound (P2)	infeasible	feasible	feasible

The effect of λ on the feasibility and optimality of a minimizer of (P3) with respect to (P1) was next evaluated. We first solved (P2) to obtain a lower bound $f(\tilde{\mathbf{d}}_2)$ on f_1. As a heuristic for setting λ, we computed $S := \sum_{t=1}^{T} \sum_{(m,n)\in\bar{\mathcal{P}}_a} c_{mn}(d_{mn}^t)^2$ from the minimizer of (P2), and chose $\lambda = 1$ so that λS was approximately $f(\tilde{\mathbf{d}}_2)/100$. For $\lambda = 1$, the minimizer of (P3) was feasible for (P1) and provided an upper bound for f_1. To tighten (2.33), problem (P3) was solved for decreasing values of λ obtaining the results of Table 2.1. The minimizer of (P3) for $\lambda = 0.1$ was feasible for (P1) and attained the same pumping cost as $f(\tilde{\mathbf{d}}_2)$. Hence,

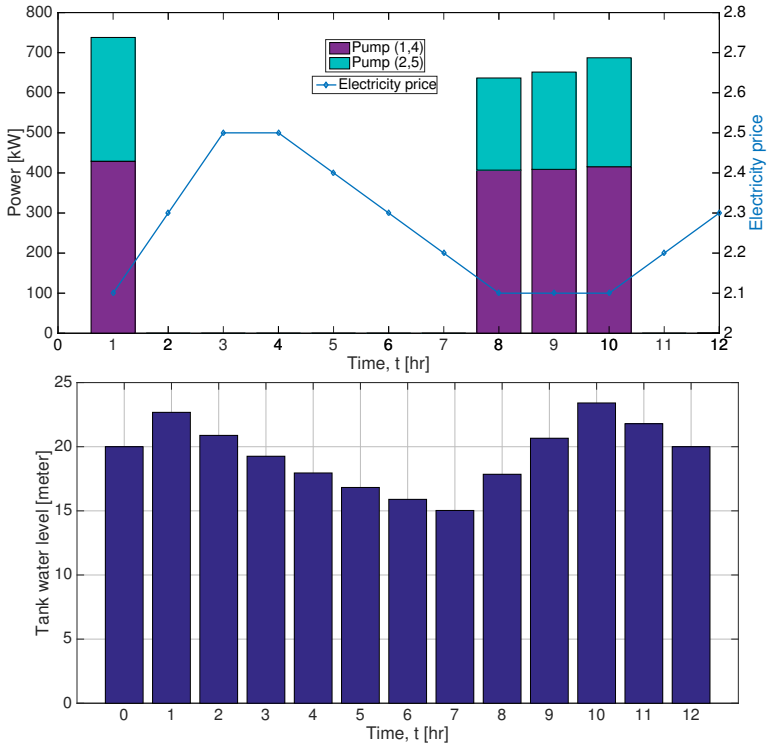

Figure 2.4: *Top:* Power drawn by pumps during hour t. Pumps $(1,4)$ and $(2,5)$ were turned on during the same hours of lower electricity prices, whereas pump $(3,7)$ was not operated. Albeit the two pumps add the same pressure gain, they exhibit different electricity consumption due to different water flows. *Bottom*: Water level in tank node 10 at the end of hour t.

the minimizer of (P3) constitutes a minimizer for (P1) as well. Heed that even though the benchmark WDS of Figure 2.2 does not meet the conditions of Lemma 2.5 and Theorem 2.6, an exact relaxation has been achieved.

Similar tests were conducted for the PJM prices between March 10–19, 2018 during 5:00–17:00; see Fig. 2.5. The results are summarized in Table 2.2. For all 10 days, problem (P3) succeeded in finding a feasible point for the values of λ reported in Table 2.2. Moreover, the upper and lower bounds $f(\tilde{\mathbf{d}}_3)$ and $f(\tilde{\mathbf{d}}_2)$ were close implying small suboptimality gaps. It is worth stressing that the relaxation in (P2) was *inexact* for all tests. Albeit cost $f(\tilde{\mathbf{d}}_2)$ was equal to $f(\tilde{\mathbf{d}}_3)$ and hence the optimal cost f_1 for some cases, there was no way to obtain a

Table 2.2: Suboptimality gap attained by feasible points obtained through (P3)

Date (Mar'18)	10	11	12	13	14	15	16	17	18	19
$f(\tilde{\mathbf{d}}_2)$	$6,968.5$	$6,915.0$	$8,524.6$	$8,404.6$	$8,220.5$	$7,237.9$	$7,206.8$	$6,807.4$	$6,404.0$	$7,206.8$
$f(\tilde{\mathbf{d}}_3)$	$7,042.8$	$7,010.9$	$8,524.6$	$8,404.6$	$8,461.8$	$7,264.7$	$7,206.8$	$6,807.4$	$6,527.1$	$7,206.8$
$\frac{f(\tilde{\mathbf{d}}_3)-f(\tilde{\mathbf{d}}_2)}{f(\tilde{\mathbf{d}}_2)}$ [%]	1.06	1.39	$7 \cdot 10^{-9}$	$3 \cdot 10^{-7}$	2.93	0.37	$2 \cdot 10^{-7}$	$7. \cdot 10^{-4}$	1.92	$2 \cdot 10^{-7}$
λ	5	5	0.5	1	10	2	0.2	0.83	6	0.6
Sol. time [min:sec]	00 : 07	21 : 00	00 : 09	00 : 06	22 : 19	00 : 29	00 : 10	00 : 51	20 : 50	00 : 18

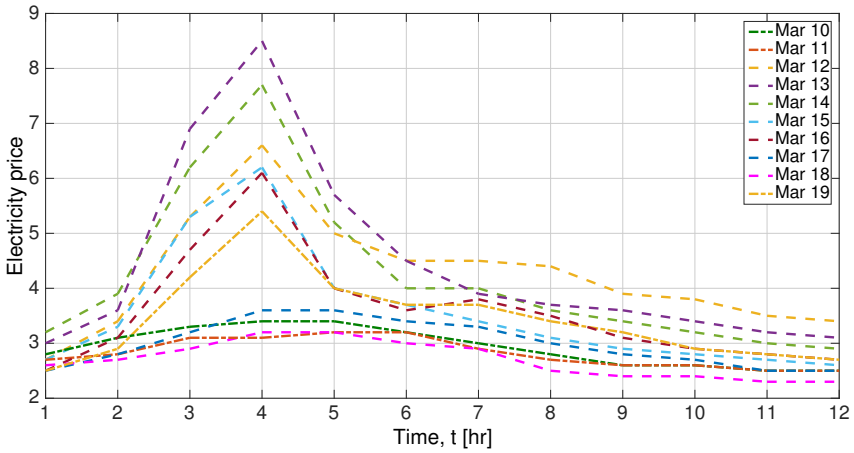

Figure 2.5: Day-ahead PJM electricity prices [¢/kWh] for March 10–19, 2018.

feasible dispatch from the minimizer of (P2).

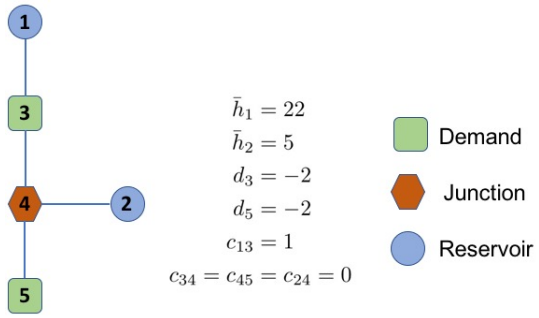

Figure 2.6: A simple WDS for which the relaxation is inexact.

To provide an example of inexact relaxation, we built the WDS of Figure 2.6. Problem (P3) and the OWF scheme of [33] were solved on this WDS for minimum pressures at nodes 3, 4, and 5, set to 6, 0, and 0. This setup features a unique feasible point: Since all edges but $(1, 3)$ are lossless, nodes 2–5 must have equal pressures. Because $\underline{h}_3 = 6$ m, the second reservoir

Table 2.3: Inexact relaxation with the WDS of Fig. 2.6

Variable	(P3)	OWF in [33]	(P1)
h_1	10	10	22
h_2	5	5	6
h_3	6	6	6
h_4	5	5	6
h_5	5	5	6
d_{13}	2	2	4
d_{34}	0	0	2
d_{24}	2	2	0
d_{45}	2	2	2
comment	inexact	inexact	optimal

with $\bar{h}_2 = 5$ m cannot supply water, the entire demand must be fulfilled by reservoir 1. This feasible point is shown in Table 2.3, along with the minimizers of (P3) and [33]. Both relaxed schemes yielded an infeasible point for (P1). The solver of [33] was not tested on the 10-node WDS earlier because it presumes: *i)* variable-speed pumps with speeds that can reach zero; and *ii)* that once a solution $(\tilde{\mathbf{d}}, \mathbf{d})$ is found, a feasible pressure $\mathbf{h}$ can be always obtained.

2.7 Optimal Water Flow: Maximizing Service Time During Power Outage

The water distribution utilities need pumps that are generally driven by electric motors, to overcome the pressure drop due to friction and to transport water uphill. Oftentimes, there is enough water stored in elevated water tanks to supply consumer demands and maintain the minimum pressure requirement, even without running the pumps. Thus, the utilities run the water pumps only for few hours in a day. In section 2.3, the pump running times were scheduled optimally to minimize the overall energy cost.

In this section, we aim at finding optimal operational strategies for water utilities during

partial/complete power outages. Outages in power distribution systems are inevitable and could range from single-line outages caused by faults to widespread outages due to extreme events [15], [16]. The damages and disruptions caused during such outages could spread beyond the power network and affect essential services like water distribution, transport, healthcare etc. However, such disruptions may not be immediate. For instance, once a water utility loses power, it still might have some stored water in elevated water tanks that can be used to serve the water demands. In this scenario, finding the optimal operational strategy by the water utilities during partial or complete power outages is a critical problem. While partial power outages affect the operation of some of the pumps in water networks, a complete power outage implies that no pump can be turned on.

The objective of the proposed OWF is maximizing the time for which a water utility can continue serving its customers once a power outage has occurred. The OWF problem involves mixed-integer quadratic equalities emancipating from the pressure drop equations. Therefore, to efficiently solve the OWF problem, an MI-SOCP relaxation, similar to section 2.4, is proposed. Numerical tests demonstrate that the relaxed problem yields exact solution for all of the numerous problem instances considered. Such performance motivates for detailed analytical investigation that can establish conditions for guaranteed exactness. However, such investigation is left for future research.

The solution sought from the problem being formulated is the maximum time $t \in \{1, \ldots, T\}$, for which all the constraints of the OWF problem (P1) may be satisfied. However, in doing so, constraint (2.10) equating the initial and final tank levels is relaxed because restoring the water-level in tank is not a priority during outages. To control the activation of different constraints during service, introduce binary variables $\{y_t\}_{t=1}^{T}$ such that $y_t = 1$ indicates that the water utility can provide service during time t; and vice versa. Considering that the objective is to maximize the total service time $\sum_{t=1}^{T} y_t$, the OWF problem can be formulated

as:

$$\min \quad -\sum_{t=1}^{T} y_t \tag{2.34}$$

$$\text{s.to} \quad (2.4),\ (2.6a)-(2.6c),\ (2.7),\ (2.8),\ (2.9),\ (2.11)$$

$$d_m^t y_t = \sum_{k:(m,k)\in\mathcal{P}} d_{mk}^t - \sum_{k:(k,m)\in\mathcal{P}} d_{km}^t, \quad \forall m,t \tag{2.35}$$

$$h_m^t \geq \underline{h}_m y_t - M(1-y_t), \quad \forall m,t \tag{2.36}$$

$$y_t \geq y_{t-1}, \quad \forall\ t \tag{2.37}$$

$$x_{mn}^t \in \{0,1\}, \quad \forall (m,n)\in\mathcal{P}_a^s;\ x_{mn}^t = 0, \quad \forall (m,n)\in\mathcal{P}_a \setminus \mathcal{P}_a^s. \tag{2.38}$$

Reviewing the constraints in problem (2.34), constraint (2.35) is the nodal flow conservation if the water service is on $y_t = 1$, else the demand served is zero and constraint (2.35) is trivially satisfied with zero flows. Constraint (2.36) enforces the minimum nodal pressure requirement during service ($y_t = 1$), and is trivially satisfied when the service is unavailable ($y_t = 0$). Constraint (2.37) enforces the operational constraint implying that the service duration is maximized in *continuation*, i.e., once the service is discontinued, it is considered as end of the service period. Remaining constraints include the mixed-integer Darcy-Weisbach equation from (2.4); the pump-model from (2.6), where (2.38) provide flexibility in operation of pumps that have power service $\mathcal{P}_a^s$, and turn off the pumps with no power service; the reservoir model (2.7); and the constraints on tank operation (2.8)-(2.9), (2.11).

As observed in section 2.3, the mixed-integer Darcy-Weisbach equation from (2.4) are non-convex even after fixing the binary variables. Thus, a penalized relaxation similar to section 2.5 is proposed next where (2.4) is replaced with (2.13) to solve the OWF in (2.34).

The penalized relaxation is formulated as

$$\begin{aligned} \min \quad & -\sum_{t=1}^{T} y_t + \lambda \sum_{(m,n)\in\bar{\mathcal{P}}_a} |h_m - h_n| \\ \text{s.to} \quad & (2.6a) - (2.6c),\ (2.7),\ (2.8),\ (2.9),\ (2.11),\ (2.13),\ (2.35) - (2.38) \end{aligned} \tag{2.39}$$

where $\lambda \geq 0$ is a tuning parameter for the penalty term. Problem (2.39) is an MI-SOCP and can be solved using off the shelf solvers. We skip a formal and rigorous analysis on the feasibility and optimality of the penalized relaxation in (2.39) for the original problem (2.34). Rather, the performance is empirically tested on the benchmark water distibution system shown in Figure 2.2. The numerical tests are discussed next.

2.7.1 Numerical Tests

The new OWF formulation was evaluated on the benchmark WDS shown in Figure 2.2. All the pipeline parameters, minimum pressure requirements, and tank dimensions were kept same as that used in Section 2.6. The WDS in Figure 2.2 consists of 3 fixed-speed pumps, all of which were assumed to be turned off due to complete power outage. As before, the tank at node 10 has water level limits $\underline{\ell}_{10} = 10$ and $\overline{\ell}_{10} = 30$ m. The tuning parameter for penalty was set to $\lambda = 10^{-3}$ for all tests in this section.

The WDS was scheduled hourly for a horizon of $T = 12$ hours for the demands of Figure 2.3. The OWF tests were solved using the MATLAB-based optimization toolbox YALMIP along with the mixed-integer solver CPLEX [44], [46]. All tests were run on a 2.7 GHz, Intel Core i5 computer with 8 GB RAM. The OWF was solved for different initial tank levels and the maximum service time obtained is shown on Figure 2.7. It may be observed that the maximum service time is zero for initial tank levels less than 22 m and rises steeply

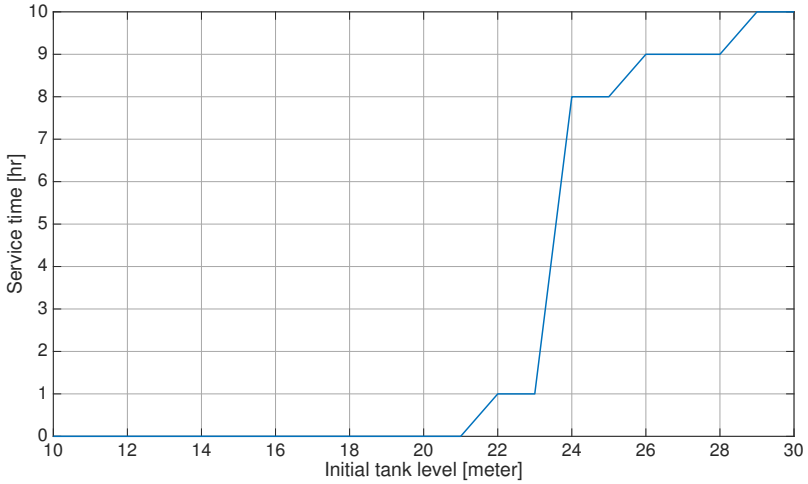

Figure 2.7: Maximum service time for different initial tank level, $\ell_{10} \in [10, 30]$.

after that. Such trend may be attributed to the high water demands in the initial hours of Figure 2.3, followed by a low demand region. It was found that even for the maximum tank level of 30m, the demand for the WDS could not be served for the entire scheduling period of 24 hours. The maximum inexactness as defined in Section 2.6, was found to be of the order of 10^{-4} for all tests, while the solving time was between $[1.73,\ 61.97]$ sec with a median of 5.87 sec.

2.8 Water Flow Problem

Different from the OWF task where the operation of tanks and pumps is scheduled over a time horizon to serve objectives such as minimizing the electricity cost, or maximizing service time during power outages, the water flow (WF) problem simply solves the equations governing the flows in a WDS. The latter task is needed in everyday WDS operations and planning. However, the non-convex quadratic pressure drop equations make the problem hard and traditional methods rely on Newton-Raphson (NR) based methods, see for example [25]. A critical limitation of NR-based approaches is the requirement of an initialization

point, which may not be trivial in general. While solving the WF problem for day-to-day operation, a good initialization point may be found from experience, or using previous system states. However, finding good initialization points remains complex for planning studies and contingency analysis. Recently, a fixed-point iteration based WF solver has been proposed in [47]. However, the applicability of the developed solver is limited to water networks without pumps, which is quite restrictive. In this section, a convex-relaxation based WF solver is developed that can accommodate pumps, as well. The WF problem is formally introduced next and an MI-SOCP relaxation is provided.

The WF problem is solved for a single time instance and thus the equations to be solved include the conservation of flow (2.1), the pressure drop equations (2.4) and the pressure added by on pumps (2.5). Formally, given the water demands at consumer nodes; water injections at reservoirs and tanks; pump statuses; and the pressure at a reference node, the WF task aims at finding all pipe flows and nodal pressures. It can be posed as

$$\text{find} \quad \{\tilde{\mathbf{d}}, \mathbf{d}, \mathbf{h}\} \tag{2.40}$$

$$\text{s.to} \quad d_m = \sum_{k:(m,k)\in\mathcal{P}} d_{mk} - \sum_{k:(k,m)\in\mathcal{P}} d_{km}, \quad \forall m, \tag{2.41}$$

$$-M(1-x_{mn}) \leq d_{mn} \leq M x_{mn}, \quad \forall (m,n) \in \bar{\mathcal{P}}_a, \tag{2.42}$$

$$-M(1-x_{mn}) \leq h_m - h_n - c_{mn}(d_{mn})^2 \leq M(1-x_{mn}), \quad \forall (m,n) \in \bar{\mathcal{P}}_a, \tag{2.43}$$

$$-M x_{mn} \leq h_m - h_n + c_{mn}(d_{mn})^2 \leq M x_{mn}, \quad \forall (m,n) \in \bar{\mathcal{P}}_a, \tag{2.44}$$

$$x_{mn} \in \{0,1\}, \quad \forall (m,n) \in \bar{\mathcal{P}}_a, \tag{2.45}$$

$$h_n - h_m = g_{mn}, \quad \forall (m,n) \in \mathcal{P}_a, \text{with } x_{mn} = 1, \tag{2.46}$$

$$h_m = h_n, \quad \forall (m,n) \in \mathcal{P}_a, \text{with } x_{mn} = 0, \tag{2.47}$$

where constraint (2.41) enforces the flow conservation; (2.42)-(2.45) represent the pressure

drop constraints (2.4) for single time instant; and (2.46)-(2.47) represent the pressure added by on and off pumps, respectively. Problem (2.40) is solved for a single time instant. In addition, pressure bounds are checked after solving the WF task, rather than imposed as constraints.

The non-convex quadratic inequalities in (2.43)-(2.44) make the WF problem (2.40) hard to solve. In line with the convex relaxation (2.13), the double-sided inequalities in (2.43)-(2.44) may be relaxed to

$$-M(1 - x_{mn}) \leq h_m - h_n - c_{mn}(d_{mn})^2 \tag{2.48a}$$

$$h_m - h_n + c_{mn}(d_{mn})^2 \leq M x_{mn}. \tag{2.48b}$$

To attain an exact relaxation from (2.48), a penalization may be introduced as in section 2.5. A similar formulation has been employed to solve the steady state natural gas flow problem in [48]. Thus the following MI-SOCP problem may be formulated to surrogate the feasibility problem (2.40)

$$\begin{aligned} \min \quad & \sum_{(m,n)\in\bar{\mathcal{P}}_a} |h_m - h_n| \\ \text{s.to} \quad & (2.41),\ (2.42),\ (2.45) - (2.47),\ (2.48), \end{aligned} \tag{2.49}$$

where the cost of (2.49) sums up the absolute pressure differences across lossy pipes. Drawing parallels from the OWF problem (P3), the results of Corollary 2.7 translate to the following claim.

Corollary 2.9. *Under the assumptions of Theorem 2.6, a minimizer of* (2.49) *is feasible for the WF problem* (2.40).

While the assumptions of Theorem 2.6 are restrictive, a WDS network grossly violating

these assumptions is used to assess the performance of the penalized relaxation of (2.49). The numerical tests are discussed next.

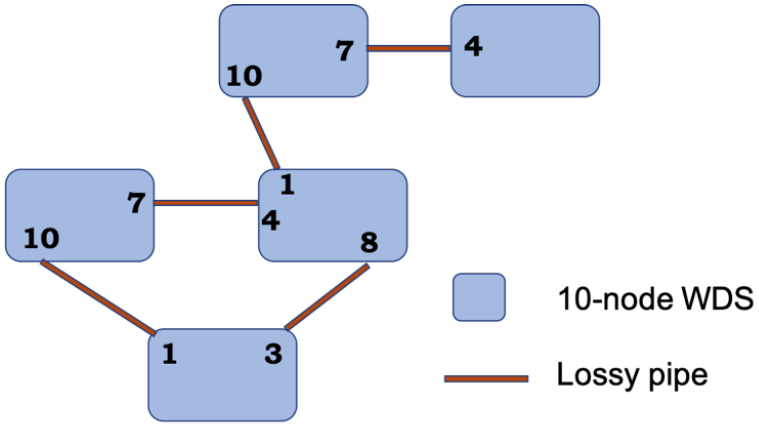

Figure 2.8: A 50-node WDS built upon connecting 5 copies of the WDS of Fig. 2.2.

2.8.1 Numerical Tests

We studied the use of (2.49) for solving the WF problem. To this end, a 50-node WDS was constructed by connecting 5 copies of the 10-node WDS of Figure 2.2 as shown in Figure 2.8. We randomly generated 500 feasible instances of the WF problem in (2.40) upon fixing pressure $h_1 = 10$ m and drawing the remaining pressures independently as Gaussian random variables of mean 10 m and variance 2 m^2, or $\mathcal{N}(10, 2)$. The statuses of pumps were drawn as independent Bernoulli random variables with equal probabilities for being on or off. If pump (m, n) was selected to be on, the pressure at its receiving node was updated as $h_n := h_m + g_{mn}$. The water flow in all lossy pipes was calculated from the so obtained pressures and the Darcy-Weisbach equation in (2.3). Flows within pumps were drawn from $\mathcal{N}(200, 20)$, with positive direction for operating pumps and random direction for off pumps. Once the complete flow vector was obtained, the injections were computed from (2.41), thus yielding random placement of water withdrawals and injections over the meshed WDS of

Fig. 2.8. The obtained vector of injections and pressure h_1 served as a feasible input for the WF task.

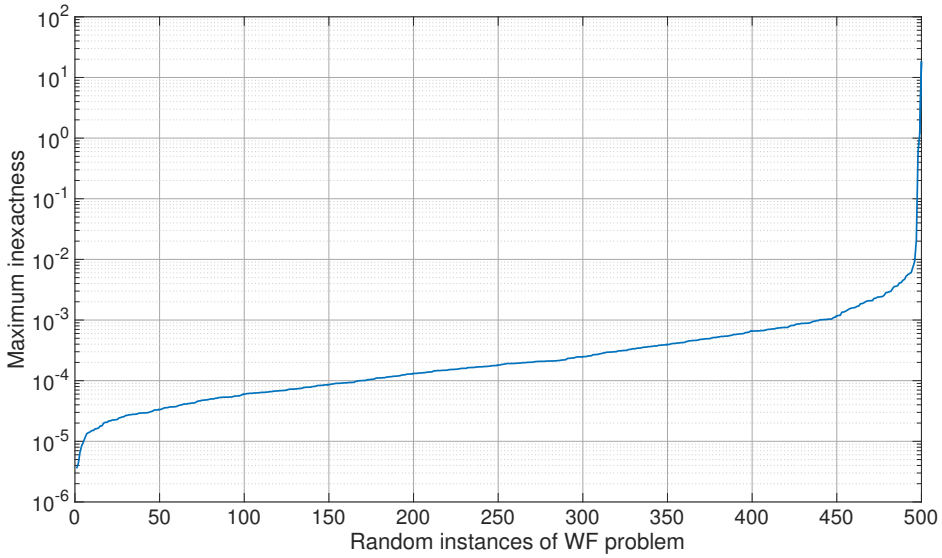

Figure 2.9: Maximum inexactness for 500 random instances of the WF task.

Problem (2.49) was solved using YALMIP and CPLEX [46]. Given a minimizer of (2.49), we defined the inexactness over lossy pipe (m, n) as $|h_m - h_n| - c_{mn}d_{mn}^2$. For each run of (2.49) with a random input, the maximum inexactness over all lossy pipelines is shown on Figure 2.9. For 90% of the cases, the maximum inexactness was less than 1.1×10^{-3}. Further, the maximum solving time over all 500 cases was found to be 6.56 sec and median time was 2.35 sec. Despite the restrictive conditions of Lemma 2.5 and Theorem 2.6, the penalized relaxation developed for the WF problem performs well. We also conducted 500 similar WF tests on the 10-node WDS of Figure 2.2. Even though, the 10-node WDS does not satisfy the conditions for Lemma 2.5 and Theorem 2.6, the maximum inexactness over all 500 random cases was 1.5×10^{-3}.

2.9 Conclusions

To cater a more adaptive WDS operation, optimal pump scheduling has been formulated here as an OWF task. Different from existing formulations, the developed OWF model includes critical pressure constraints capturing the operation of tanks, reservoirs, pipes, and valves. The original mixed-integer non-convex problem has been modified to a mixed-integer second-order cone program over a relaxed feasible set. Moreover, its objective augmented by a judiciously designed penalty term, so that under specific conditions, this modified problem can recover minimizers of the original problem. Numerical tests validate that by properly tuning the penalization parameter λ, the modified problem solves the original one over different water demand and electricity pricing setups.

The developed penalized relaxation approach has been further used for two practical tasks: *i)* Solving an OWF problem that maximizes the time for which a water utility can continue service in an event of a power outage in the area; *ii)* Solving the WF problem. The novel formulation towards optimal operation of a WDS during power outages can incorporate partial and complete power outages alike. Numerical tests demonstrate that the relaxed MI-SOCP yields exact solutions within seconds for the benchmark WDS. Similarly, the numerical tests for the proposed MI-SOCP based WF solver demonstrate that it scales well for moderately sized water distribution networks. While the analytical conditions for exactness are restrictive, the numerical tests show that the developed formulation yields exact relaxation even when the assumptions are grossly violated. The favorable optimality and feasibilty of the minimizers of the two relaxed problems motivate for more rigorous analytical investigation. Finding explicit conditions for exactness and bounds on suboptimality constitutes our future research. Generalizing the developed penalized relaxation approach towards scheduling variable-speed pumps, coupled WDS–electric power distribution network

operation, incorporating stochasticity in future water demands constitute pertinent research directions.

Chapter 3

Optimal Power Distribution System Restoration

Note: Reproduced from Reference [14]

3.1 Introduction

Outages in power distribution systems are inevitable and could range from single-line outages caused by faults to widespread outages due to extreme events [15], [16]. Extreme events in the form of natural disasters, accidents, or cyber attacks, could result in a tremendous loss of distribution infrastructure [17], [18]. Meticulously designing the response to outages could significantly improve system resiliency [49]. Conventionally, distribution system restoration was predominantly manual, and was based on trouble calls, the operator's prior experience, and field search crews. Currently, the rampant deployment of smart meters, grid sensors, and controlled switches, offers improved situational awareness and remote control [50]. To expedite grid restoration, many efforts have been put towards its automation based on available resources.

The task of distribution system restoration (DSR) is initiated after the post-outage status of the distribution grid has been assessed. Operators traditionally resort to network reconfiguration schemes to limit the impact of an outage while satisfying operational and design

constraints. The DSR task is typically formulated as a combinatorially complex non-linear minimization. Traditionally, it has been approached using dynamic programming [51]; expert systems [52]; fuzzy logic [53]; genetic algorithms [54]; and mixed-integer non-linear programming [55]. Nonetheless, with the advent of distributed generators (DG) and microgrids, new challenges and opportunities have been introduced in the DSR problem.

Distributed generators and microgrids could enable islanded operation, thus improving resiliency against extreme events. The coordinated operation of heterogeneous DGs introduces different operational and control requirements [56]. Although several recent works deal with DGs and microgrids [18], [57], [58], [59]; they all presume that each DG features black-start capability and/or preclude running multiple DGs on the same island. The former does not hold for solar DGs without energy storage. The latter over-simplifies the operational capabilities of DGs and thus constitutes a restriction of the actual DSR task. Albeit [16] allows for multiple DGs operating on the same island, their control mode is decided through a suboptimal two-stage process. In a nutshell, a realistic coordination of DGs and microgrids for DSR remains largely under-explored.

This work puts forth a novel system restoration scheme with three major improvements over existing alternatives: *i)* Our DSR scheme finds the optimal formation of islands in a single stage, different from prior works that first identify reference generators and then build islands around them; *ii)* It further allows for multiple (non)-black-start DGs running on the same island and decides their optimal coordination; and *iii)* It devises an exact model for voltage regulators. Through the novel use of cycles and paths on the grid infrastructure graph, and by leveraging the McCormick linearization and an approximate grid model, our optimal DSR task can be posed as an MILP, which scales well on a moderately-sized feeder.

3.2 Preliminaries

Before defining the DSR task, we review some preliminaries from graph theory and the McCormick linearization. Consider an undirected graph $\mathcal{G} := (\mathcal{N}, \mathcal{E})$ with $\mathcal{N}$ being its node set and $\mathcal{E}$ its edge set. The graph is connected if there exists a sequence of adjacent edges between any two of its nodes. A *path* from node i to j is defined as the sequence of edges $\mathcal{P}_{ij}$ starting at node i and terminating at node j. A *cycle* is a sequence of adjacent edges without repetition that starts and ends at the same node. A *tree* is a connected graph with no cycles. If every edge $e \in \mathcal{E}$ is assigned a direction, the obtained graph is termed *directed*.

As a brief review, the McCormick linearization is a widely used technique for handling products of optimization variables $x_1 x_2 \cdot x_N$ by their linear convex envelopes [60]. Since this relaxation is not necessarily exact, there is a rich literature on tightening approaches; see for example [61] and references therein. In fact, the McCormick linearization becomes exact for the special case of bilinear terms involving at least one binary variable: Consider the constraint $z = xy$, according to which the variable z equals the the binary variable $x \in \{0, 1\}$ times the continuous variable y. If y is constrained within $y \in [\underline{y}, \bar{y}]$, the constraint $z = xy$ can be equivalently expressed by the four linear inequality constraints

$$x\underline{y} \leq z \leq x\bar{y}, \tag{3.1a}$$

$$y + (x-1)\bar{y} \leq z \leq y + (x-1)\underline{y}. \tag{3.1b}$$

The equivalence can be readily verified by observing that for $x = 1$, constraint (3.1b) yields $z = y$ and (3.1a) holds trivially. When $x = 0$, both (3.1a) and (3.1b) yield $z = 0$. Combining the two cases provides $z = xy$ indeed. Henceforth, all bilinear products of binary and (bounded) continuous variables could be handled by the McCormick linearization of (3.1).

3.3 Problem Formulation

During an outage, protection devices isolate certain parts of a distribution system including the faulty elements. While replacing faulty elements may be time-consuming, remotely-controlled switches could reconfigure the system to alleviate the outage effect. Given the post-fault status, the *single-step DSR* task finds the grid topology that minimizes the outage impact while complying with operational constraints. The presumption is that the system transitions instantaneously from the post-fault to the final condition. In practice, this transition is implemented via a sequence of reconfiguration steps involving one control action at a time. Due to space limitations, here we consider the single-step DSR task on a single-phase grid model.

A distribution system can be represented by a graph $\mathcal{G} := (\mathcal{N}, \mathcal{E})$. Its nodes are indexed by $i \in \mathcal{N} := \{0, \ldots, N\}$ correspond to buses, and its edges $\mathcal{E}$ to distribution lines, switches, and voltage regulators. An edge running between nodes i and j is assigned an arbitrary direction, and is denoted as $e : (i, j)$ or $e : (j, i) \in \mathcal{E}$. Although multiple islands may be formed by opening switches, graph $\mathcal{G}$ is connected since the distribution system is structurally connected.

3.3.1 Nodal Variables and Constraints

Each bus $i \in \mathcal{N}$ hosts at most one generator or load. This is without loss of generality since a bus with multiple loads can be modeled as a set of single-load buses, all connected by non-switchable zero-impedance lines. Moreover, to ensure that all substations remain disconnected from each other, they are combined into a single root node indexed by 0 as in [57]. The power limit of a substation can be imposed as a limit on the line connecting the substation with its feeder. To simplify the exposition, on-load tap changers (OLTCs)

are ignored and all substations are assumed to operate at the nominal voltage.

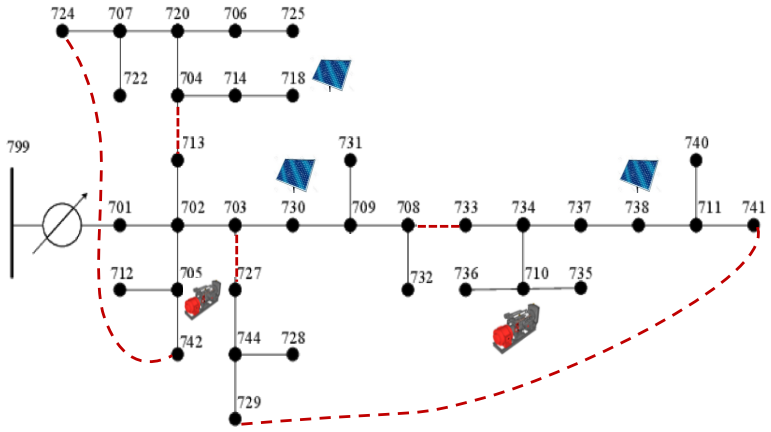

Figure 3.1: A modified IEEE 37-bus feeder showing existing lines and generators.

To capture which buses are energized, introduce the vector of bus statuses $\mathbf{x} \in \{0,1\}^{|\mathcal{N}|}$. Its i-th entry equals 1 if bus i is energized, and 0 otherwise. If v_i is the squared voltage magnitude and $p_i + jq_i$ the complex power injection on bus i, we enforce the constraints

$$x_i \in \{0,1\}, \qquad \forall\, i \in \mathcal{N} \tag{3.2a}$$

$$x_i \underline{v}_i \leq v_i \leq x_i \bar{v}_i, \qquad \forall\, i \in \mathcal{N} \tag{3.2b}$$

$$x_i \underline{p}_i \leq p_i \leq x_i \bar{p}_i, \qquad \forall\, i \in \mathcal{N} \tag{3.2c}$$

$$x_i \underline{q}_i \leq q_i \leq x_i \bar{q}_i, \qquad \forall\, i \in \mathcal{N}. \tag{3.2d}$$

Constraint (3.2b) ensures that voltages remain within voltage regulation limits for energized buses (e.g., $\pm 3\%$ per unit); and set voltages to zero for non-energized buses. The substation voltage can be set by selecting $\underline{v}_0 = \bar{v}_0 = v_0$. Constraints (3.2c)–(3.2d) limit the complex power injections at energized nodes. The signed values for $\{\underline{p}_i, \bar{p}_i, \underline{q}_i, \bar{q}_i\}$ determine whether an injection corresponds to a generator; a fixed load with lagging or leading power factor; or an elastic load.

Not all DGs have black-start capabilities [62]: For instance, rooftop solar generators without

energy storage can generate power only if the corresponding bus is already energized. On the other hand, diesel and gas-fired generators may feature black-start and grid-forming capabilities. To capture this functionality, define $\mathcal{S}_B \subseteq \mathcal{N}$ as the set of buses hosting black-start generators, and $\mathcal{S}_{NB} \subseteq \mathcal{N}$ as the set of buses with non-black-start generators.

3.3.2 Edge Variables and Constraints

Let us now partition the set of edges $\mathcal{E}$ into:

- the subset $\mathcal{E}_O$ of out-of-service lines;
- the subset $\mathcal{E}_I$ of in-service lines;
- the subset $\mathcal{E}_S$ of switches; and
- the subset $\mathcal{E}_R$ of in-service voltage regulators.

Since non-remotely controlled switches cannot participate in DSR, they are handled as lines and belong to $\mathcal{E}_I$. Figure 3.1 depicts a feeder hosting 3 solar generators; 2 black-start diesel generators; 5 switches; and 1 voltage regulator.

Similar to buses, the vector of edge statuses $\mathbf{y} \in \{0,1\}^{|\mathcal{E}|}$ indicates which edges are closed. Vector $\mathbf{y}$ should satisfy

$$y_e \in \{0,1\}, \qquad \forall\ e \in \mathcal{E}_S \tag{3.3a}$$

$$y_e = 0, \qquad \forall\ e \in \mathcal{E}_O \tag{3.3b}$$

$$y_e = 1, \qquad \forall\ e \in \mathcal{E}_I \cup \mathcal{E}_R \tag{3.3c}$$

$$y_e \underline{P}_e \leq P_e \leq y_e \bar{P}_e, \qquad \forall\ e \in \mathcal{E} \tag{3.3d}$$

$$y_e \underline{Q}_e \leq Q_e \leq y_e \bar{Q}_e, \qquad \forall\ e \in \mathcal{E} \tag{3.3e}$$

where $P_e + jQ_e$ is the complex flow on line e. Power flow limits are typically set as $\underline{P}_e = -\bar{P}_e$ and $\underline{Q}_e = -\bar{Q}_e$.

Even though apparent flow limits of the form $P_e^2 + Q_e^2 \leq S_e^2$ can be added to our formulation, they result in a mixed-integer quadratic program, which does not scale as gracefully as an MILP. Alternatively, apparent constraints on line flows and bus injections can be handled by a polytopic inner or outer approximation of $P_e^2 + Q_e^2 \leq S_e^2$; see e.g., [63]. This approach is not adopted here to keep the formulation uncluttered.

3.3.3 Voltage Drops and Regulators

To relate power injections, power flows, and voltages, we adopt the *linearized distribution flow* (LDF) model [64]–[65]. Albeit approximate, the LDF model has been engaged in various grid optimization tasks with satisfactory accuracy [66]. Given the complexity and uncertainty involved in DSR, the approximation error incurred by LDF becomes inconsequential.

Upon ignoring ohmic losses on lines, the LDF model expresses bus injections as

$$p_i = \sum_{e:(i,j)\in\mathcal{E}} P_e - \sum_{e:(j,i)\in\mathcal{E}} P_e, \quad \forall\, i \in \mathcal{N} \tag{3.4a}$$

$$q_i = \sum_{e:(i,j)\in\mathcal{E}} Q_e - \sum_{e:(j,i)\in\mathcal{E}} Q_e, \quad \forall\, i \in \mathcal{N}. \tag{3.4b}$$

Constraint (3.4) essentially imposes the complex power balance at each node. For node $i = 0$, it implies that the injected power equals the total power withdrawn by the feeder.

According to the LDF model, the voltage drop along line e with impedance $r_e + jx_e$ can be approximated as

$$y_e \left(v_i - v_j - 2r_e P_e - 2x_e Q_e\right) = 0, \ \forall\, e : (i,j) \in \mathcal{E} \setminus \mathcal{E}_R. \tag{3.5}$$

The drop occurs only if line e is closed ($y_e = 1$); and (3.5) is not enforced for voltage regulators.

Constraint (3.5) involves the bilinear terms $y_e v_i$, $y_e v_j$, $y_e P_e$, and $y_e Q_e$. As discussed in Section 3.2, each one of these products can be replaced by an auxiliary variable, so that (3.5) can be posed as a linear equality constraint relating the four auxiliary variables. The auxiliary variable associated with $y_e v_i$ is related to y_e and v_i via four linear inequalities as in (3.1). The same holds for the other three bilinear terms. Luckily, the McCormick linearization is used scarcely, since only a few edges represent switches.

We proceed with voltage regulators, which are modeled as ideal. This is without loss of generality since the impedance of a non-ideal regulator can be modeled as a line connected in series with the ideal regulator. A regulator can scale its secondary-side voltage by $\pm 10\%$ by increments of 0.625% using tap positions [67]. The taps can be changed either remotely, or based on some automated control usually based on local voltage (and current) measurements. Due to space limitations, all regulators are assumed to be remotely controlled.

Consider regulator $r : (i, j) \in \mathcal{E}_R$. Its voltage transformation ratio can be set to $1+0.00625 \cdot t_r$, where $t_r \in \{0, \pm 1, \ldots, \pm 16\}$ is its tap position. The transformation in terms of squared voltage magnitudes is

$$v_j = (1 + 0.00625 \cdot t_r)^2 v_i. \tag{3.6}$$

The quadratic dependence on t_r is often replaced by a linear approximation [68]. Waiving this approximation, we pursue a simple yet *exact* regulator model: The term in the parenthesis of (3.6) can take one out of 33 possible values. These values are collected in vector $\mathbf{c} \in \mathbb{R}^{33}$ whose k-th entry is $c_k := [1 + 0.00625 \cdot (k - 17)]^2$. Vector $\mathbf{c}$ is known beforehand and is common for all regulators. By introducing the tap status vectors $\mathbf{t}_r$, the operation of regulators is

modeled as

$$v_j = v_i \cdot \mathbf{t}_r^\top \mathbf{c}, \qquad \forall\, r : (i,j) \in \mathcal{E}_R \tag{3.7a}$$

$$\mathbf{t}_r \in \{0,1\}^{33}, \qquad \forall\, r : (i,j) \in \mathcal{E}_R \tag{3.7b}$$

$$\mathbf{t}_r^\top \mathbf{1} = 1, \qquad \forall\, r : (i,j) \in \mathcal{E}_R. \tag{3.7c}$$

There is only one non-zero entry in $\mathbf{t}_r$ due to (3.7c). The bilinear product in (3.7a) can be handled via the McCormick scheme.

3.3.4 Topological Constraints

To deal with network constraints, let us introduce indicator vectors for paths and cycles. Because $\mathcal{G}$ is connected, there exists at least one path for each pair of nodes i and j. For path $\mathcal{P}$, define its indicator vector $\boldsymbol{\pi}^{\mathcal{P}} \in \{0,1\}^{|\mathcal{E}|}$, such that $\pi_e^{\mathcal{P}} = 1$ if $e \in \mathcal{P}$, and $\pi_e^{\mathcal{P}} = 0$ otherwise. In essence, vector $\boldsymbol{\pi}^{\mathcal{P}}$ indicates which edges comprise $\mathcal{P}$, regardless their directionality. Similarly, for any cycle $\mathcal{C}$ in $\mathcal{G}$, define the cycle indicator vector $\mathbf{n}^{\mathcal{C}} \in \{0,1\}^{|\mathcal{E}|}$, such that $n_e^{\mathcal{C}} = 1$ if $e \in \mathcal{C}$, and $n_e^{\mathcal{C}} = 0$ otherwise.

Distribution grids are typically operated in a tree (radial) structure to ease protection coordination. To enforce radiality, previous works were confined to unidirectional power flows [57]. Anticipating increasing penetration of renewables, we facilitate radiality even with reverse flows. To avoid the formation of cycles, we add the constraint

$$\mathbf{y}^\top \mathbf{n}^{\mathcal{C}} \leq \mathbf{1}^\top \mathbf{n}^{\mathcal{C}} - 1, \quad \forall \mathcal{C} \tag{3.8}$$

for all cycles $\mathcal{C}$ in $\mathcal{G}$. Constraint (3.8) limits the number of closed edges along cycle $\mathcal{C}$ to be less than the total number of edges in $\mathcal{C}$. Due to the limited number of switches, there

are few cycles $\mathcal{C}$. For instance, the system of Figure 3.1 has five switches giving rise to two cycles.

In addition, if line $e : (i, j) \in \mathcal{E}$ is closed, the buses i and j must share the same status (both energized or not)

$$|x_i - x_j| \leq 1 - y_e, \quad \forall\ e : (i, j) \in \mathcal{E}. \tag{3.9}$$

3.3.5 Coordinating Generators

Non-black-start generators (e.g., rooftop photovoltaics) can generate power only when they are connected to a substation or a running black-start generator; see [18], [62]. If there exists such path for generator $i \in \mathcal{S}_{NB}$, then constraint (3.9) implies $x_i = 1$. Otherwise, the status $x_i = 0$ must be enforced explicitly. To this end, identify all paths from generator $i \in \mathcal{S}_{NB}$ to all $j \in \mathcal{S}_B$. These paths are denoted by $\mathcal{P}_{i,k}$ for $k = 1, \ldots, K_i$ and all $i \in \mathcal{S}_{NB}$; there are 21 such paths in the feeder of Fig. 3.1. For path $\mathcal{P}_{i,k}$, let $\boldsymbol{\pi}_{i,k}$ be its indicator vector and introduce the binary variable $\delta_{i,k}$ for which

$$\delta_{i,k} \in \{0, 1\}, \qquad \forall \mathcal{P}_{i,k} \tag{3.10a}$$

$$\delta_{i,k} \cdot \mathbf{1}^\top \boldsymbol{\pi}_{i,k} \leq \mathbf{y}^\top \boldsymbol{\pi}_{i,k}, \qquad \forall \mathcal{P}_{i,k} \tag{3.10b}$$

$$x_i \leq \sum_k \delta_{i,k}, \qquad \forall i \in \mathcal{S}_{NB}. \tag{3.10c}$$

By definition of the indicator vector $\boldsymbol{\pi}_{i,k}$, we have that $\mathbf{y}^\top \boldsymbol{\pi}_{i,k} \leq \mathbf{1}^\top \boldsymbol{\pi}_{i,k}$ with equality only if path $\mathcal{P}_{i,k}$ is energized. If $\mathcal{P}_{i,k}$ is *not* energized, then (3.10a)–(3.10b) imply $\delta_{i,k} = 0$. If $\mathcal{P}_{i,k}$ is energized, then $\delta_{i,k}$ can be either 0 or 1; yet bus i is guaranteed to be energized by applying (3.9) along $\mathcal{P}_{i,k}$. Constraint (3.10c) entails that for bus i to be energized, at least one of the paths $\{\mathcal{P}_{i,k}\}_k$ is energized. In other words, each non-black-start DG can run only if it is

connected to a running black-start DG or a substation.

When an island includes multiple black-start DGs, a simple coordination scheme is that the largest DG i operates in PV mode ($v_i = v_0$), and the rest in PQ mode [62]. Moreover, if black-start DGs operate in grid-connected mode, the substation should be treated as the largest generator and all DGs operate in PQ mode. To model this, identify all paths between each $i \in \mathcal{S}_B$ and all generators $j \in \mathcal{S}_B$ of larger rating. These paths are denoted by $\mathcal{L}_{i,\ell}$ and indexed by $\ell = 1, \ldots, L_i$ for $i \in \mathcal{S}_B$; there are 8 such paths in the feeder of Fig. 3.1. The indicator vector for path $\mathcal{L}_{i,\ell}$ is denoted by $\boldsymbol{\ell}_{i,l}$. For each $\mathcal{L}_{i,\ell}$, introduce the variable $\epsilon_{i,\ell}$, which equals 1 if $\mathcal{L}_{i,\ell}$ is energized; and 0, otherwise. With the help of $\epsilon_{i,\ell}$'s, the coordination of generators can be captured by

$$\epsilon_{i,\ell} \in \{0, 1\}, \qquad \forall \mathcal{L}_{i,\ell} \tag{3.11a}$$

$$(\mathbf{y} - \mathbf{1})^\top \boldsymbol{\ell}_{i,l} + 1 \leq \epsilon_{i,\ell} \leq \frac{\mathbf{y}^\top \boldsymbol{\ell}_{i,l}}{\mathbf{1}^\top \boldsymbol{\ell}_{i,l}}, \qquad \forall \mathcal{L}_{i,\ell}. \tag{3.11b}$$

If path $\mathcal{L}_{i,\ell}$ is energized, then $\mathbf{y}^\top \boldsymbol{\ell}_{i,l} = \mathbf{1}^\top \boldsymbol{\ell}_{i,l}$, and (3.11) entails $\epsilon_{i,\ell} = 1$. If $\mathcal{L}_{i,\ell}$ is not energized, then $\mathbf{y}^\top \boldsymbol{\ell}_{i,l} < \mathbf{1}^\top \boldsymbol{\ell}_{i,l}$. Because $\mathbf{y}^\top \boldsymbol{\ell}_{i,l}$ counts the number of closed lines in $\mathcal{L}_{i,\ell}$, it holds $\mathbf{y}^\top \boldsymbol{\ell}_{i,l} \leq \mathbf{1}^\top \boldsymbol{\ell}_{i,l} - 1$ and so (3.11) entails $\epsilon_{i,\ell} = 0$.

To model the operation mode for generator $i \in \mathcal{S}_B$, introduce variable ϵ_i that equals 1 if the generator operates in PQ, and 0 when in PV mode. Using $\epsilon'_{i,\ell}s$, the coordination of generator modes is accomplished as

$$\epsilon_i \in \{0, 1\}, \qquad \forall i \in \mathcal{S}_B \tag{3.12a}$$

$$\max_\ell \epsilon_{i,\ell} \leq \epsilon_i \leq \sum_\ell \epsilon_{i,\ell}, \qquad \forall i \in \mathcal{S}_B \tag{3.12b}$$

$$|v_i - v_0| \leq \epsilon_i v_0, \qquad \forall i \in \mathcal{S}_B. \tag{3.12c}$$

Constraint (3.12b) ensures that if any of the paths $\{\mathcal{L}_{i,\ell}\}_\ell$ is energized, then $\epsilon_i = 1$ and (3.12c) follows trivially due to voltage regulation. This scenario means that generator i is connected to a larger black-start generator or the substation, and hence operates in PQ mode. On the other hand, if $\epsilon_{i,\ell} = 0$ for all ℓ, generator i is the largest on the island. In this case, constraint (3.12b) yields $\epsilon_i = 0$, and (3.12c) sets $v_i = v_0$.

3.3.6 Objective Function

Let vectors $\mathbf{x}^0$ and $\mathbf{y}^0$ represent the post-outage statuses of nodes and lines. A meaningful restoration objective is to find a grid topology $\mathbf{y}$ and generation dispatch that maximize the total served load. Among several restoration schemes, an operator may prefer the schemes with fewer line switching operations. Moreover, a usual practice dictates that the restoration process must not de-energize an already energized bus. The DSR problem can be now formulated as

$$\min \sum_{i \in \mathcal{N} \setminus (\mathcal{S}_B \cup \mathcal{S}_{NB} \cup \{0\})} p_i + \lambda \mathbf{1}^\top |\mathbf{y} - \mathbf{y}^0| \tag{3.13}$$

$$\text{s.to} \quad (3.9) - (3.12), \mathbf{x} \geq \mathbf{x}^0 \tag{3.14}$$

where parameter $\lambda \geq 0$ quantifies the importance of restoration schemes with fewer switching operations. Setting $\lambda = 0$ yields the scheme with the maximum load served. Problem (3.13) is an MILP and can be solved by off-the-shelf solvers.

3.4 Numerical Tests

The developed DSR approach was tested on a modified version of the IEEE 37-node feeder converted to its single-phase equivalent [69]; see Figure 3.1. Two black-start DGs of capacities 459.3 and 918.5 kW were placed on nodes 705 and 710, respectively. Three non-black-start DGs were placed on buses 718, 730, and 738 with capacities set to half the load on the associated buses. The switchable lines include 3 existing and two additional lines shown as dashed. The (re)active loads on buses 701, 722, 737, and 738 were elastic with their minimum set to half the nominal bus load. All tests were run using MATLAB-based toolbox YALMIP along with the mixed-integer solver CPLEX [44], [46]; on a 2.7 GHz Intel Core i5 computer with 8 GB RAM; and for $\lambda = 10^{-3}$.

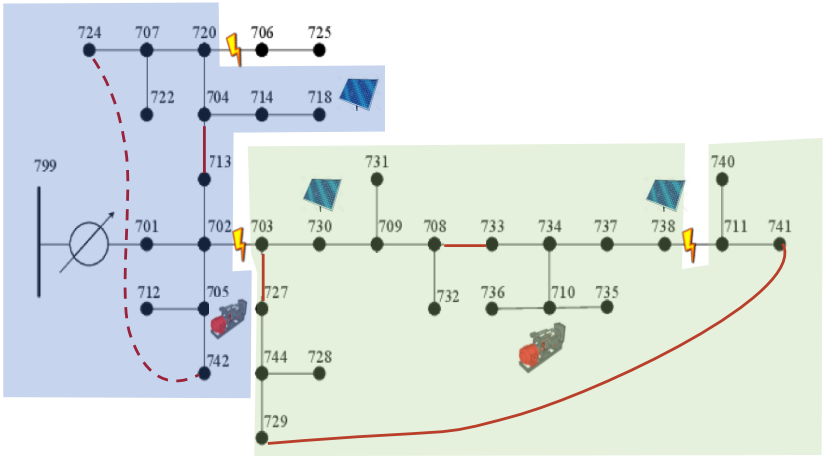

Figure 3.2: The feeder of Figure 3.1 restored after a 3-line outage.

The performance of our DSR scheme was tested for an outage scenario of three line outages shown in Figure 3.2. The restored system comprises of two sub-networks, while buses 706 and 725 could not be restored. The DG on bus 710 serves as the reference bus for the second island.

The computational performance of the MILP in (3.13) was tested using $1,000$ random outage scenarios, 200 scenarios for each number of $1-5$ lines in outage. The maximum available

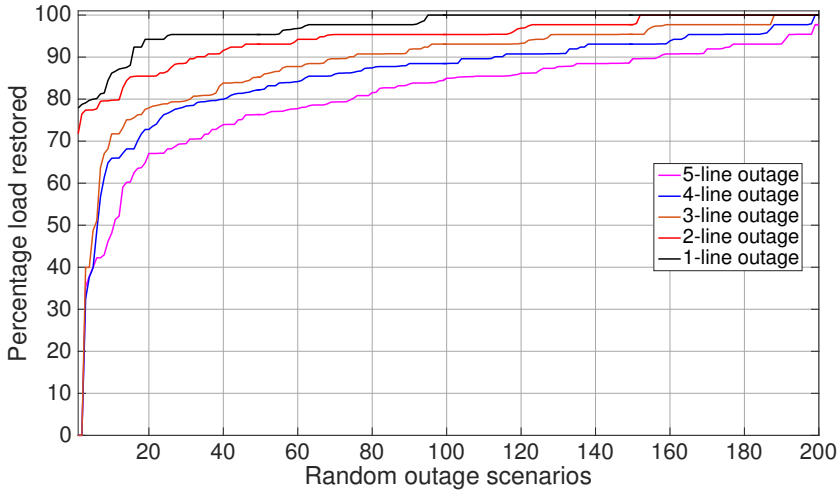

Figure 3.3: The (ordered) percentage of load restored after 1–5 line outages.

solar generations were drawn from a uniform distribution based on the respective rated sizes. The running times for solving (3.13) reported in Table 3.1 demonstrate that our DSR scales well for single- and multiple-line outages alike. The percentage load restored for the various line outages is shown (ordered) in Figure 3.3. As anticipated, the total load restored decreases as the number of outages increases.

Table 3.1: Running times for the MILP of (3.13)

Number of outaged lines	1	2	3	4	5
Maximum running time [sec]	1.04	0.96	2.69	3.96	1.77
Median running time [sec]	0.79	0.78	0.77	0.81	0.73

3.5 Conclusions

The developed DSR scheme features optimal formation of islands; incorporates voltage regulators; allows for multiple DGs on each island and establishes a coordination hierarchy amongst them. Numerical tests demonstrate the correctness of the MILP formulation and that its complexity scales well in moderately-sized feeders. Its scalability can be attributed

to three key points: *i)* the unique use of indicator vectors for cycles and paths over the infrastructure graph; *ii)* the McCormick linearization; and *iii)* the approximate LDF model. Although framed within the DSR paradigm, this work sets the solid foundations for several grid optimization tasks including reconfiguration for power loss minimization and Volt/VAR control. We are currently working towards extending this scheme to its multi-step variant; incorporating switched capacitor banks and locally-controlled voltage regulators; and considering unbalanced multi-phase feeders.

Chapter 4

Summary and Future Work

A computationally efficient frameworks towards analysis and operation of water and power distribution networks individually, and in cohesion has been developed in this thesis. The various problems addressed in this thesis are in general non-convex, even on fixing the discrete decision variables. Thus, convex relaxations have been proposed to make the problems tractable. Moreover, novel penalty terms have been designed tp promote exact relaxations. Next, analytical guarantees for exactness have been found under pre-defined conditions. The developed formulations are shown to apply to a broader class of practical problems. Relaxing the assumptions laid in Chapters **??**-3 and further generalizing the developed framework is a natural subject of future research. Specifically, our pertinent research efforts include:

- Incorporating variable speed pumps in the developed (optimal) water flow framework.
- The generalized OWF formulations developed in this thesis motivate us towards coupled optimization and scheduling of water and power networks.
- The WF problem in Section 2.8 yields exact solution numerically even when the identified assumptions are violated. This motivates us towards analytically relaxing the assumptions.
- The OWF of Section 2.7 is a modified special case of the OWF of Section 2.3. Hence further analysis may help in relaxing the stringent conditions found for the OWF of Section 2.3.

- The DSR scheme developed in Chapter 3 finds an optimal final topology for load restoration. However, in practice, restoration is a sequential activity with time-coupling constraints such as ramping, monotonic energization of nodes, cold-load pick-up, finite energy storage and maximum down-times. Thus, developing a sequential T-time step DSR scheme with consideration of power system dynamics constraints constitutes our current research efforts.

Bibliography

[1] S. P. Mohanty, U. Choppali, and E. Kougianos, "Everything you wanted to know about smart cities: The internet of things is the backbone," *IEEE Consumer Electronics Magazine*, vol. 5, no. 3, pp. 60–70, Jul. 2016.

[2] R. R. Harmon, E. G. Castro-Leon, and S. Bhide, "Smart cities and the internet of things," in *Proc. 2015 Portland Int. Conf. on Management of Eng. and Tech.*, Aug. 2015, pp. 485–494.

[3] B. N. Silva, M. Khan, and K. Han, "Towards sustainable smart cities: A review of trends, architectures, components, and open challenges in smart cities," *Sustainable Cities and Society*, vol. 38, pp. 697–713, Apr. 2018.

[4] A. Ojha, "Coupled natural gas and electric power systems," Master's thesis, Virginia Tech, 2017.

[5] A. Martinez-Mares and C. R. Fuerte-Esquivel, "A unified gas and power flow analysis in natural gas and electricity coupled networks," *IEEE Trans. Power Syst.*, vol. 27, no. 4, pp. 2156–2166, Nov. 2012.

[6] A. Zlotnik, L. Roald, S. Backhaus, M. Chertkov, and G. Andersson, "Coordinated scheduling for interdependent electric power and natural gas infrastructures," *IEEE Trans. Power Syst.*, vol. 32, no. 1, pp. 600–610, Jan. 2017.

[7] E. Casey, S. Beaini, S. Pabi, K. Zammit, and A. Amarnath, "The triple bottom line for efficiency: Integrating systems within water and energy networks," *IEEE Power and Energy Magazine*, vol. 15, no. 1, pp. 34–42, Jan. 2017.

[8] K. Oikonomou, M. Parvania, and S. Burian, "Integrating water distribution energy flexibility in power systems operation," in *Proc. IEEE PES General Meeting*, Chicago, IL, Jul. 2017.

[9] K. Oikonomou, M. Parvania, and R. Khatami, "Optimal demand response scheduling for water distribution systems," *IEEE Trans. Ind. Informat.*, 2018, (early access).

[10] J. Lin, S. Sedigh, and A. Miller, "A general framework for quantitative modeling of dependability in cyber-physical systems: A proposal for doctoral research," in *Proc. 33rd Annual IEEE Int. Comp. Software and Applications Conf.*, vol. 1, Jul. 2009, pp. 668–671.

[11] H. Mala-Jetmarova, N. Sultanova, and D. Savic, "Lost in optimisation of water distribution systems? A literature review of system operation," *Environmental Modelling & Software*, vol. 93, pp. 209–254, 2017.

[12] M. K. Singh and V. Kekatos, "Optimal scheduling of water distribution systems," *IEEE Trans. Control of Network Systems*, 2018, (submitted). [Online]. Available: http://arxiv.org/abs/1806.07988

[13] A. Atamtürk and V. Narayanan, "Conic mixed-integer rounding cuts," *Mathematical Programming*, vol. 122, no. 1, pp. 1–20, Mar. 2010.

[14] M. K. Singh, V. Kekatos, and C.-C. Liu, "Optimal distribution system restoration with microgrids and distributed generators," submitted to IEEE Power and Energy Society General Meeting (PES-GM)., Atlanta, GA, Aug. 2019. [Online]. Available: https://arxiv.org/abs/1811.04147

[15] C. Chen, J. Wang, and D. Ton, "Modernizing distribution system restoration to achieve

grid resiliency against extreme weather events: An integrated solution," *Proc. IEEE*, vol. 105, no. 7, pp. 1267–1288, Jul. 2017.

[16] Y. Wang, Y. Xu, J. He, C.-C. Liu, K. P. Schneider, M. Hong, and D. T. Ton, "Coordinating multiple sources for service restoration to enhance resilience of distribution systems," 2018. [Online]. Available: https://arxiv.org/abs/1810.06907

[17] Y. Wang, C. Chen, J. Wang, and R. Baldick, "Research on resilience of power systems under natural disasters – A review," *IEEE Trans. Power Syst.*, vol. 31, no. 2, pp. 1604–1613, Mar. 2016.

[18] B. Chen, C. Chen, J. Wang, and K. L. Butler-Purry, "Sequential service restoration for unbalanced distribution systems and microgrids," *IEEE Trans. Power Syst.*, vol. 33, no. 2, pp. 1507–1520, Mar. 2018.

[19] H. D. Sherali, R. Totlani, and G. Loganathan, "Enhanced lower bounds for the global optimization of water distribution networks," *Water Resources Research*, vol. 34, no. 7, pp. 1831–1841, Jul. 1998.

[20] H. D. Sherali, S. Subramanian, and G. Loganathan, "Effective relaxations and partitioning schemes for solving water distribution network design problems to global optimality," *J. of Global Optimization*, vol. 19, no. 1, pp. 1–26, Jan. 2001.

[21] Z. W. Geem, "Optimal cost design of water distribution networks using harmony search," *Engineering Optimization*, vol. 38, no. 3, pp. 259–277, 2006.

[22] C. DAmbrosio, A. Lodi, S. Wiese, and C. Bragalli, "Mathematical programming techniques in water network optimization," *European J. of Operational Research*, vol. 243, no. 3, pp. 774 – 788, Jun. 2015.

[23] D. Denig-Chakroff, "Reducing electricity used for water production: Questions state commissions should ask regulated utilities," *Water Research and Policy*, Jun. 2008.

[24] J. E. Van-Zyl, D. A. Savic, and G. A. Walters, "Operational optimization of water distribution systems using a hybrid genetic algorithm," *J. of Water Resources Planning and Management*, vol. 130, no. 2, pp. 160–170, 2004.

[25] L. A. Rossman, "EPANET 2 user's manual," 2000.

[26] F. K. Odan, L. F. R. Reis, and Z. Kapelan, "Real-time multiobjective optimization of operation of water supply systems," *J. Water Resour. Plann. Manage.*, vol. 141, no. 9, p. 04015011, Sep. 2015.

[27] S. S. Hashemi, M. Tabesh, and B. Ataeekia, "Ant-colony optimization of pumping schedule to minimize the energy cost using variable-speed pumps in water distribution networks," *Urban Water J.*, vol. 11, no. 5, pp. 335–347, 2014.

[28] B. Ghaddar, J. Naoum-Sawaya, A. Kishimoto, N. Taheri, and B. Eck, "A Lagrangian decomposition approach for the pump scheduling problem in water networks," *European J. of Operational Research*, vol. 241, no. 2, pp. 490 – 501, Mar. 2015.

[29] D. R. Broad, H. R. Maier, and G. C. Dandy, "Optimal operation of complex water distribution systems using metamodels," *J. of Water Resources Planning and Management*, vol. 136, no. 4, pp. 433–443, 2010.

[30] Y. Arai, A. Koizumi, T. Inakazu, A. Masuko, and S. Tamura, "Optimized operation of water distribution system using multipurpose fuzzy LP model," *Water Science & Technol.*, vol. 13, no. 1, pp. 66–73, 2013.

[31] C. Giacomello, Z. Kapelan, and M. Nicolini, "Fast hybrid optimization method for

effective pump scheduling," *J. of Water Resources Planning and Management*, vol. 139, no. 2, pp. 175–183, 2013.

[32] B. J. Eck and M. Mevissen, "Valve placement in water networks: Mixed-integer non-linear optimization with quadratic pipe friction," *IBM Research Rep.*, 2012.

[33] D. Fooladivanda and J. A. Taylor, "Optimal pump scheduling and water flow in water distribution networks," in *Proc. IEEE Conf. on Decision and Control*, Osaka, Japan, Dec. 2015, pp. 5265–5271.

[34] ——, "Energy-optimal pump scheduling and water flow," *IEEE Trans. Control of Network Systems*, vol. PP, no. 99, pp. 1–1, 2017.

[35] A. Ferdowsi, A. Sanjab, W. Saad, and N. B. Mandayam, "Game theory for secure critical interdependent gas-power-water infrastructure," in *Proc. Resilience Week*, Wilmington, USA, Sep. 2017, pp. 184–190.

[36] D. Verleye and E.-H. Aghezzaf, "Optimising production and distribution operations in large water supply networks: A piecewise linear optimisation approach," *Intl. J. of Production Research*, vol. 51, no. 23-24, pp. 7170–7189, 2013.

[37] A. S. Zamzam, E. Dall'Anese, C. Zhao, J. A. Taylor, and N. Sidiropoulos, "Optimal water-power flow problem: Formulation and distributed optimal solution," *IEEE Trans. Control of Network Systems*, vol. PP, no. 99, pp. 1–1, 2018.

[38] K. Oikonomou and M. Parvania, "Optimal coordination of water distribution energy flexibility with power systems operation," *IEEE Trans. Smart Grid*, 2018, (early access).

[39] R. Menke, E. Abraham, P. Parpas, and I. Stoianov, "Extending the envelope of demand response provision through variable speed pumps," *Procedia Engineering*, vol. 186, pp. 584 – 591, 2017.

[40] B. Ulanicki, J. Kahler, and B. Coulbeck, "Modeling the efficiency and power characteristics of a pump group," *J. of Water Resources Planning and Management*, vol. 134, no. 1, pp. 88–93, 2008.

[41] D. Cohen, U. Shamir, and G. Sinai, "Optimal operation of multi-quality water supply systems-II: The Q-H model," *Engineering Optimization*, vol. 32, no. 6, pp. 687–719, 2000.

[42] C. Godsil and G. Royle, *Algebraic Graph Theory*. New York, NY: Springer, 2001.

[43] S. Boyd and L. Vandenberghe, *Convex Optimization*. New York, NY: Cambridge University Press, 2004.

[44] J. Lofberg, "YALMIP: a toolbox for modeling and optimization in MATLAB," in *IEEE Intl. Conf. on Robotics and Automation*, New Orleans, LA, Sep. 2004, pp. 284–289.

[45] Gurobi Optimization, Inc., "Gurobi optimizer reference manual," 2016. [Online]. Available: http://www.gurobi.com

[46] IBM Corp., "Ibm ilog cplex optimization studio cplex user's manual," 2017. [Online]. Available: http://www.ibm.com

[47] M. Bazrafshan, N. Gatsis, M. Giacomoni, and A. Taha, "A fixed-point iteration for steady-state analysis of water distribution networks," 2018. [Online]. Available: arXivpreprintarXiv:1807.01404

[48] M. K. Singh and V. Kekatos, "Natural gas flow equations: Uniqueness and an MI-SOCP solver," 2018. [Online]. Available: https://arxiv.org/abs/1809.09025

[49] D. T. Ton and W. P. Wang, "A more resilient grid: The U.S. Department of Energy joins with stakeholders in an R&D plan," *IEEE Power Energy Mag.*, vol. 13, no. 3, pp. 26–34, May 2015.

[50] C. Abbey, D. Cornforth, N. Hatziargyriou, K. Hirose, A. Kwasinski, E. Kyriakides, G. Platt, L. Reyes, and S. Suryanarayanan, "Powering through the storm: Microgrids operation for more efficient disaster recovery," *IEEE Power Energy Mag.*, vol. 12, no. 3, pp. 67–76, May 2014.

[51] R. Perez-Guerrero, G. T. Heydt, N. J. Jack, B. K. Keel, and A. R. Castelhano, "Optimal restoration of distribution systems using dynamic programming," *IEEE Trans. Power Delivery*, vol. 23, no. 3, pp. 1589–1596, Jul. 2008.

[52] C.-C. Liu, S. J. Lee, and S. S. Venkata, "An expert system operational aid for restoration and loss reduction of distribution systems," *IEEE Trans. Power Syst.*, vol. 3, no. 2, pp. 619–626, May 1988.

[53] S. I. Lim, S. J. Lee, M. S. Choi, D. J. Lim, and B. N. Ha, "Service restoration methodology for multiple fault case in distribution systems," *IEEE Trans. Power Syst.*, vol. 21, no. 4, pp. 1638–1644, Nov. 2006.

[54] I. Watanabe and M. Nodu, "A genetic algorithm for optimizing switching sequence of service restoration in distribution systems," in *Proc. 2004 Cong. Evol. Comput.*, vol. 2, June 2004, pp. 1683–1690.

[55] S. Khushalani, J. M. Solanki, and N. N. Schulz, "Optimized restoration of unbalanced distribution systems," *IEEE Trans. Power Syst.*, vol. 22, no. 2, pp. 624–630, May 2007.

[56] F. Katiraei and M. R. Iravani, "Power management strategies for a microgrid with multiple distributed generation units," *IEEE Trans. Power Syst.*, vol. 21, no. 4, pp. 1821–1831, Nov. 2006.

[57] J. Li, X. Ma, C.-C. Liu, and K. P. Schneider, "Distribution system restoration with

microgrids using spanning tree search," *IEEE Trans. Power Syst.*, vol. 29, no. 6, pp. 3021–3029, Nov. 2014.

[58] Z. Wang and J. Wang, "Self-healing resilient distribution systems based on sectionalization into microgrids," *IEEE Trans. Power Syst.*, vol. 30, no. 6, pp. 3139–3149, Nov. 2015.

[59] J. F. Franco, M. J. Rider, M. Lavorato, and R. Romero, "A mixed-integer LP model for the reconfiguration of radial electric distribution systems considering distributed generation," *Electric Power Systems Research*, vol. 97, pp. 51–60, Apr. 2013.

[60] G. P. McCormick, "Computability of global solutions to factorable nonconvex programs: Part I – Convex underestimating problems," *Mathematical Programming*, vol. 10, no. 1, pp. 147–175, Dec. 1976.

[61] H. Nagarajan, M. Lu, E. Yamangil, and R. Bent, "Tightening McCormick relaxations for nonlinear programs via dynamic multivariate partitioning," in *Principles and Practice of Constraint Programming*. Springer, Aug. 2016, pp. 369–387.

[62] C. L. Moreira, F. O. Resende, and J. A. P. Lopes, "Using low voltage microgrids for service restoration," *IEEE Trans. Power Syst.*, vol. 22, no. 1, pp. 395–403, Feb. 2007.

[63] R. A. Jabr, "Linear decision rules for control of reactive power by distributed photovoltaic generators," *IEEE Trans. Power Syst.*, vol. 33, no. 2, pp. 2165–2174, Mar. 2018.

[64] M. Baran and F. Wu, "Optimal capacitor placement on radial distribution systems," *IEEE Trans. Power Syst.*, vol. 4, no. 1, pp. 725–734, Jan. 1989.

[65] ——, "Optimal sizing of capacitors placed on a radial distribution system," *IEEE Trans. Power Syst.*, vol. 4, no. 1, pp. 735–743, Jan. 1989.

[66] V. Kekatos, L. Zhang, G. B. Giannakis, and R. Baldick, "Voltage regulation algorithms for multiphase power distribution grids," *IEEE Trans. Power Syst.*, vol. 31, no. 5, pp. 3913–3923, Sep. 2016.

[67] J. A. Kersulis and I. A. Hiskens, "Renewable voltage regulation and the transformer tapping trade-off," in *Proc. IEEE Conf. on Innovative Smart Grid Technologies*, Melbourne, Australia, Nov. 2016.

[68] J. Lopez, J. Contreras, and J. R. S. Mantovani, "Reactive power planning under conditional-value-at-risk assessment using chance-constrained optimisation," *IET Gener. Transm. Dis.*, vol. 9, no. 3, pp. 231–240, Feb. 2015.

[69] G. Cavraro, V. Kekatos, and S. Veeramachaneni, "Voltage analytics for power distribution network topology verification," *IEEE Trans. Smart Grid*, 2018, (early access).